A Nonlinear Analysis of Spatial Compliant Parallel Modules: Multi-beam Modules

Guangbo Hao, Xianwen Kong[1], Robert L. Reuben

Department of Mechanical Engineering, Heriot-Watt University, Edinburgh, UK, EH14 4AS

ABSTRACT: This paper presents normalized, nonlinear and analytical models of spatial compliant parallel modules—multi-beam modules with a large range of motion. The models address the non-linearity of load-equilibrium equations, applied in the deformed configuration, under small deflection hypothesis. First, spatial nonlinear load-displacement equations of the tip of a beam, conditions of geometry compatibility and load-equilibrium conditions for a spatial three-beam module are derived. The nonlinear and analytical load-displacement equations for the three-beam module are then solved using three methods: approximate analytical method, improved analytical method and numerical method. The nonlinear-analytical solutions, linear solutions and large-deflection FEA solutions are further analyzed and compared. FEA verifies that the accuracy of the proposed nonlinear-analytical model is acceptable. Moreover, a class of multi-beam modules with four or more beams is proposed, and their general nonlinear load-displacement equations are obtained based on the approximate load-displacement equations of the three-beam module. The proposed multi-beam modules and their nonlinear models have potential applications in the compliant mechanism design. Especially, the multi-beam modules can be regarded as building blocks of novel compliant parallel mechanisms.

***Keywords*:** Nonlinear analysis; Compliant mechanisms; Spatial modules

1. Introduction

Compliant parallel mechanisms/modules (CPMs) transmit motions/forces by deflections of their compliant members and have the characteristics of both conventional parallel mechanisms [1-2] and fully compliant mechanisms [3-4]. It is well known that CPMs possess many potential advantages such as zero backlash, no need for lubrication, reduced wear, high precision and compact, monolithic configuration. They can be used in a variety of applications, especially where high-precision movements are required, such as precision motion stages, precision robotics, and MEMS sensors and actuators [5-8]. Due to their merits, CPMs have received much attention over the past decade.

CPMs mainly fall into two categories: lumped compliance mechanisms and distributed compliance mechanisms. Compared to lumped compliant joints, distributed compliant joints can produce a large range of motion as well as a reduced stress concentration, and their elastic averaging can permit inexact constraint designs. There are three main approaches to design of compliant mechanisms: (a) Pseudo-Rigid-Body-Model synthesis methods [9-11], (b) Continuum Structure Optimization methods [12-14], and (c) innovative design methods such as the constraint-based design approach [15-16], the building block approach [17], the screw theory based approach and the freedom and constraint topology approach [18-20].

Traditional linear analysis or Pseudo-Rigid-Body-Models [4] have limited application for compliant mechanisms usually only providing an initial estimate for displacements as a reference for nonlinear analysis. Non-linearities in force-displacement characteristics of a basic cantilever beam (*Euler-Bernoulli* beam) have three sources: material non-linearity, geometric non-linearity and non-linearity of load-equilibrium equations. The material non-linearity can be neglected for most applications and the geometric non-linearity will also be ignored in this paper due to small deflection assumption. To capture the nonlinearities of force-displacement equations, the load-equilibrium conditions should be applied in the deformed configuration of compliant mechanisms [5, 21-22], which is different from the configuration before deformation as used in linear load-equilibrium. There are two main methods of solving force-displacement equations: a) differential equation based methods [5, 23], and b) energy methods, such as Castigliano's theorem [24, 25] and virtual work principle [4]. Awtar [5] has derived the analytical and nonlinear force-displacement equations of a basic cantilever beam of length L in matrix form under the small deflection assumption, which applies provided that the transverse displacement is less than $0.1L$. These nonlinear equations can be directly used to define the buckling conditions and capture the effects of load-stiffening and elastokinematic nonlinearities, both resulting from axial forces in the beams [5, 26]. Zelenika *et al* [22] also proposed the nonlinear equations of a leaf spring in the cross-spring pivot in the deformed configuration. Nevertheless, these equations can not be generally used due to the limitation of derivation, and the complication of solution using numerical method. Awtar *et al* [27, 23] further studied the elastic averaging effect in multi-beam parallelogram flexure mechanisms, analyzed the characteristics of a double parallelogram flexure module and proposed simple and accurate approximations. This body of work revealed the fact that any difference in the axial forces acting on the beams will cause an unequal transverse stiffness change in the beams, and result in rotational yaw. Based on the contributions in [15], Hao and Kong [28] proposed a 3-DOF (degrees of freedom) CPM for translation. This CPM has good characteristics such as the kinematostatic-decoupling and large range of motion.

This paper builds on the above advances, and investigates the nonlinear modeling of spatial CPMs with multiple *Euler-Bernoulli* beams under small deflection and plane cross-section assumption. A multi-beam module is composed of a motion stage and a base connected using three or more slender beams [3, 5]. In addition to being an independent CPM in its own right, e.g. as a vibratory bowl feeder [29-30] and a compliant assembly system device [31], a multi-beam module can also be used as building blocks of new spatial compliant mechanisms [32-33]. This offers an alternative to spatial CPMs composed of a number of planar compliant modules with distributed compliance, which have been proposed elsewhere [23, 34-35]. Dai *et al* [29] have already analyzed the compliance of a three-legged rigidly connected compliant platform using screw theory using the *linear* compliance matrix for each leg. Ding *et al* [30] have also carried out a dynamic analysis of a vibratory bowl feeder with three spatial compliant legs based on a characteristic equation. Recently, a tilted three-beam spatial compliant module, producing three rotations, is analyzed to define layouts of actuators using screw theory [36]. However, as yet, there has been no analysis of a spatial module with three or more uniform non-tilted slender beams.

[1]Corresponding author, Phone: +44(0)1314513688, Email address: X.Kong@hw.ac.uk

Accordingly, this paper focuses on multi-beam modules with uniform non-tilted beams (Fig. 1). The reasons for this choice are that the uniform beam is one of the most common flexure elements and the non-tilted arrangement is simple enough to allow for closed-form analysis in terms of constraint-based design. This paper is organized as follows. In Section 2, spatial nonlinear load-displacement equations of the tip of a beam, conditions of geometry compatibility and load-equilibrium conditions of the spatial three-beam module are derived. In Section 3, three approaches are proposed to solve the nonlinear load-displacement equations for the three-beam module, and the validity condition, extensible application, accuracy and advantages/limitations of each model are discussed, and the approximate model is compared with the linear model. In Section 4, FEA is conducted to verify the proposed approximate analytical model for the three-beam module. In Section 5, a class of multi-beam spatial modules is proposed, and the general equations of load-displacement for these modules are summarized. Finally, conclusions are drawn.

2. Spatial three-beam module analysis

In order to simplify equations and make translational displacements and rotational angles (or forces and moments) comparable, all translational displacements and length parameters are normalized by the beam length L, forces by EI/L^2, bending moments by EI/L, and torques by GI_p/L. Here, E denotes the Young's modulus, I denotes the second moment of the area of a cross-section, G denotes the shear modulus, and I_p denotes the polar second moment of the area of the cross-section. Throughout the paper, non-dimensional quantities are represented by the corresponding lower-case letters, and all beams have round cross-sections with the same diameter D_0 unless otherwise indicated.

The three-beam module (Figs. 1 and 2) is composed of a base, three beams and a motion stage. The base and motion stage, which are both assumed to be rigid, are connected by the three compliant beams. Here, the three beams are uniformly spaced around a circle of radius r_3 on the base and on the motion stage, and all external loads, p (axial force), f_y, f_z (transverse forces), m_x (torque), m_y and m_z (bending moments), are acting at the centre, O', of the motion stage and cause the motion stage to move by deformation of the three beams. p, f_y and f_z are the forces along the X-, Y- and Z-axes, respectively; m_x, m_y and m_z re the moments about the X-, Y- and Z-axes, respectively. For the purpose of simplification, the gravity of the motion stage (including the payloads on it) is integrated into the axial force, and the weights of the compliant beams, which are very small, are neglected.

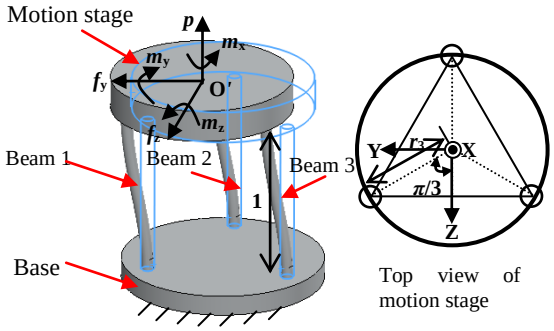

Fig. 1 Spatial three-beam module.

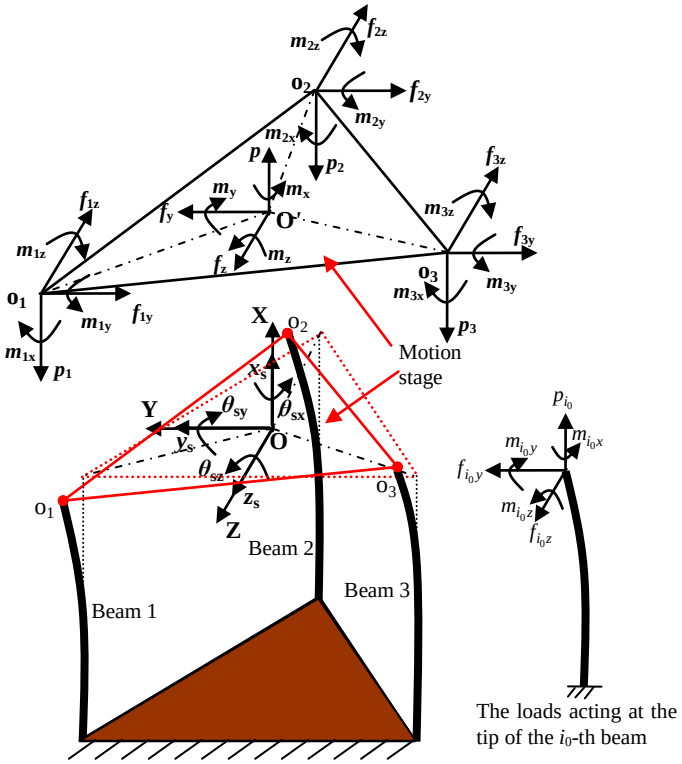

Fig. 2 Free body diagram of the spatial CPM.

In the initial configuration, a mobile rigid body coordinate system O'-X'Y'Z' and a global fixed coordinate system O-XYZ are coincident and both origins are at the centre, O', of the motion stage (Fig. 2). All translational displacements of the new origin, O', along the X-, Y- and Z-axes are denoted by x_s (axial displacement) y_s and z_s (transverse displacements), respectively; All rotational displacements (angles) of the motion stage about the X-, Y- and Z-axes are denoted by θ_{sx} (torsional angle), θ_{sy} and θ_{sz} (bending angles), respectively. All loads and displacements shown in all figures are represented by the nondimensional quantities in the coordinate system O-XYZ. The object is to investigate the translational displacements, x_s, y_s and z_s, and the rotational displacements, θ_{sx}, θ_{sy} and θ_{sz}, of the motion stage as a function of the applied loads: p, f_y, f_z, m_x, m_y and m_z.

In terms of the constraint-based design [5], the three out-of-plane DOF of the three-beam spatial module are suppressed, and its motion stage is constrained to move within the YZ plane, which leaves y_s, z_s and θ_{sx} as the DOF. If the pitch radius r_3 of the beams (hence the motion stage) becomes relatively large, the rotation of the motion stage about the X-axis will be constrained as well.

2.1. Nonlinear load-displacement equations of the tip of a cantilever beam

The centre of the free-end of the cantilever beam is used as the point (tip) at which the loads and translational movements are defined. Here, the loads, p_{i_0}, f_{i_0y}, f_{i_0z}, m_{i_0x}, m_{i_0y}, m_{i_0z} (i_0=1, 2, 3), denote internal loads acting at the tip, o_{i_0}, of the i_0-th beam, and are the corresponding reactions at the point i_0 on the motion stage as shown in Fig. 2. p_{i_0}, f_{i_0y}, f_{i_0z} are the forces along the X-, Y- and Z-axes, respectively; m_{i_0x}, m_{i_0y}, m_{i_0z} are the moments about the X-, Y- and Z-axes, respectively. θ_{i_0x}, θ_{i_0y} and θ_{i_0z} (i_0=1, 2, 3) are rotational displacements of the free-end of the i_0-th beam about the X-, Y- and Z-axes, respectively. x_{i_0}, y_{i_0} and z_{i_0} (i_0=1, 2, 3) are translational displacements of the tip of the i_0-th beam along the X-, Y- and Z-axes, respectively.

Under the conditions of linear elasticity and small deflections, the principle of superposition [24] can be applied to straightforwardly deal with the spatial combined deformation of a beam. The combined deformation can be regarded as the combination of two bending deformations in the XY and XZ planes, respectively, and a torsional deformation about the X-axis. The bending of a beam in a given plane can be analyzed using the nonlinear load-displacement equations derived by Awtar [5, 23]. An alternative derivation for the nonlinear analysis of planar deflection of a beam can also be found in Appendix A.

Equations (A. 12a) and (A. 13a) allow the nonlinear load-displacement equations for the i_0-th beam (i_0 = 1, 2, 3) for bending in the XY and XZ planes to be written as

$$\begin{bmatrix} f_{i_0y} \\ m_{i_0z} \end{bmatrix} = \begin{bmatrix} a & c \\ c & b \end{bmatrix} \begin{bmatrix} y_{i_0} \\ \theta_{i_0z} \end{bmatrix} + p_{i_0} \begin{bmatrix} e & h \\ h & g \end{bmatrix} \begin{bmatrix} y_{i_0} \\ \theta_{i_0z} \end{bmatrix} + p_{i_0}^2 \begin{bmatrix} -1/700 & 1/1400 \\ 1/1400 & -11/6300 \end{bmatrix} \begin{bmatrix} y_{i_0} \\ \theta_{i_0z} \end{bmatrix} + \cdots \tag{1}$$

and

$$\begin{bmatrix} f_{i_0z} \\ -m_{i_0y} \end{bmatrix} = \begin{bmatrix} a & c \\ c & b \end{bmatrix} \begin{bmatrix} z_{i_0} \\ -\theta_{i_0y} \end{bmatrix} + p_{i_0} \begin{bmatrix} e & h \\ h & g \end{bmatrix} \begin{bmatrix} z_{i_0} \\ -\theta_{i_0y} \end{bmatrix} + p_{i_0}^2 \begin{bmatrix} -1/700 & 1/1400 \\ 1/1400 & -11/6300 \end{bmatrix} \begin{bmatrix} z_{i_0} \\ -\theta_{i_0y} \end{bmatrix} + \cdots \tag{2}$$

where the second term on the right hand side of Eqs. (1) or (2) shows the load-stiffening effect, and the terms after the second can be neglected for most applications. Equations (1) and (2) are valid under the assumption that the moment about the Y(Z)-axis acting at any location on the beam does not affect the bending in the XY (XZ) plane, i.e. that the two bending deformations are decoupled or are weakly coupled.

The axial displacement of the i_0-th tip can be obtained by adding Eqs. (A. 12b) and (A. 13b) (contributions from bending in the XY and XZ planes) and deducting one of the duplicated terms (purely elastic effect):

$$\begin{aligned} x_{i_0} = {} & \frac{1}{d} p_{i_0} + [y_{i_0}, \theta_{i_0z}] \begin{bmatrix} i & k \\ k & j \end{bmatrix} \begin{bmatrix} y_{i_0} \\ \theta_{i_0z} \end{bmatrix} + p_{i_0} [y_{i_0}, \theta_{i_0z}] \begin{bmatrix} r & q \\ q & s \end{bmatrix} \begin{bmatrix} y_{i_0} \\ \theta_{i_0z} \end{bmatrix} + [z_{i_0}, -\theta_{i_0y}] \begin{bmatrix} i & k \\ k & j \end{bmatrix} \begin{bmatrix} z_{i_0} \\ -\theta_{i_0y} \end{bmatrix} + p_{i_0} [z_{i_0}, -\theta_{i_0y}] \begin{bmatrix} r & q \\ q & s \end{bmatrix} \begin{bmatrix} z_{i_0} \\ -\theta_{i_0y} \end{bmatrix} \\ & + p_{i_0}^2 [y_{i_0}, \theta_{i_0z}] \begin{bmatrix} 1/42000 & -1/84000 \\ -1/84000 & 1/18000 \end{bmatrix} \begin{bmatrix} y_{i_0} \\ \theta_{i_0z} \end{bmatrix} + \cdots + p_{i_0}^2 [z_{i_0}, -\theta_{i_0y}] \begin{bmatrix} 1/42000 & -1/84000 \\ -1/84000 & 1/18000 \end{bmatrix} \begin{bmatrix} z_{i_0} \\ -\theta_{i_0y} \end{bmatrix} + \cdots \end{aligned} \tag{3}$$

where the first term on the right hand side represents the purely elastic effect of the axial force alone, the second and the fourth terms show the purely kinematic effect, and the third and the fifth terms show the elastokinematic effect. For most practical situations the terms after the fifth can be ignored.

The nonlinear load-displacement equation of the i_0-th beam (i_0=1, 2, 3) for the torsion about the X-axis after deformation can be obtained (see Appendix B for detailed derivation):

$$\theta_{i_0x} = m_{i_0x} - c(\theta_{i_0z} z_{i_0} + \theta_{i_0y} y_{i_0})/\delta - p_{i_0} h(\theta_{i_0z} z_{i_0} + \theta_{i_0y} y_{i_0})/\delta \tag{4}$$

where δ=2G/E. The first term shows the purely elastic effect of the torque alone, the second term shows the purely kinematic effect, and the third term shows the elastokinematic effect. Due to the very small bending angles, compared with the transverse displacements and the torsional angle in the spatial three-beam module, we can also omit the purely kinematic and the elastokinematic effects in Eq. (4).

The coefficients a, b, c, d, e, g, h, i, j, k, q, r and s used above are all non-dimensional numbers and are the characteristic of the uniform round cross-section beam [5]:

a= 12, b= 4, c= -6, d=16/(D_0/L)^2;

e= 1.2, g= 2/15, h= -0.1;

i= -0.6, j= -1/15, k= 1/20;
r= 1/700, s= 11/6300, q= -1/1400.

From Eqs. (1) - (4), it can be seen that p_{i_0}, f_{i_0y}, f_{i_0z}, m_{i_0y} and m_{i_0z} are all approximately in the order of 1, and m_{i_0x} is in the order of 0.1 since $x_{i_0}, y_{i_0}, z_{i_0}, \theta_{i_0x}, \theta_{i_0y}, \theta_{i_0z}$ are all in the order of 0.1 under the small deflection assumption [5].

2.2. Conditions of geometric compatibility

For small absolute values of rotational angles (in the order of 0.1), the rotation sequence of three *Euler angles* is insignificant [37] and its contribution can be neglected. Due to the rigidity of the motion stage, the geometric compatibility of the rotational angles can be described:

$$\theta_{sx} = \theta_{1x} = \theta_{2x} = \theta_{3x} \tag{5a}$$

$$\theta_{sy} = \theta_{1y} = \theta_{2y} = \theta_{3y} \tag{5b}$$

$$\theta_{sz} = \theta_{1z} = \theta_{2z} = \theta_{3z} \tag{5c}$$

The translational displacement relationships between the tip of the i_0-th beam and the centre of the motion stage can be expressed as

$$\begin{bmatrix} x_{i_0} \\ y_{i_0} \\ z_{i_0} \end{bmatrix} = \begin{bmatrix} x''_{i_0} - x'_{i_0} \\ y''_{i_0} - y'_{i_0} \\ z''_{i_0} - z'_{i_0} \end{bmatrix} + \begin{bmatrix} x_s \\ y_s \\ z_s \end{bmatrix} = \begin{bmatrix} x''_{i_0} \\ y''_{i_0} \\ z''_{i_0} \end{bmatrix} + \begin{bmatrix} x_s - x'_{i_0} \\ y_s - y'_{i_0} \\ z_s - z'_{i_0} \end{bmatrix} \tag{6}$$

where x''_{i_0}, y''_{i_0} and z''_{i_0} are the coordinates of the tip of the i_0-th beam relative to the global fixed coordinate system after only the rotations of the motion stage (no movement at the point O'). x'_{i_0}, y'_{i_0} and z'_{i_0} are the local coordinates of the tip of the i_0-th beam relative to the mobile rigid body coordinate system (x'_1=0, y'_1=$r_3$sin(π/3), z'_1=$r_3$cos(π/3) for the tip 1, x'_2=0, y'_2=0, z'_2=-r_3 for the tip 2, x'_3=0, y'_3=-$r_3$sin(π/3), z'_3=$r_3$cos(π/3) for the tip 3).

The coordinates x''_{i_0}, y''_{i_0} and z''_{i_0} can be further expressed in a rotation matrix form as

$$\begin{bmatrix} x''_{i_0} \\ y''_{i_0} \\ z''_{i_0} \end{bmatrix} = \mathbf{R}_{\mathrm{Z}}(\theta_{sz})\mathbf{R}_{\mathrm{Y}}(\theta_{sy})\mathbf{R}_{\mathrm{X}}(\theta_{sx}) \begin{bmatrix} x'_{i_0} \\ y'_{i_0} \\ z'_{i_0} \end{bmatrix} \tag{7}$$

where $\mathbf{R}_{\mathrm{X}}$, $\mathbf{R}_{\mathrm{Y}}$ and $\mathbf{R}_{\mathrm{Z}}$ are the sequential rotation matrices [18] about the X-, Y- and Z-axes, respectively.

For small rotation angles, high order terms of rotational angles in the product of three rotation matrices above can be neglected, so:

$$\mathbf{R}_{\mathrm{Z}}(\theta_{sz})\mathbf{R}_{\mathrm{Y}}(\theta_{sy})\mathbf{R}_{\mathrm{X}}(\theta_{sx}) \approx \begin{bmatrix} 1 & -\theta_{sz} + \theta_{sy}\theta_{sx} & \theta_{sz}\theta_{sx} + \theta_{sy} \\ \theta_{sz} & 1 & -\theta_{sx} + \theta_{sz}\theta_{sy} \\ -\theta_{sy} & \theta_{sx} & 1 \end{bmatrix} \approx \begin{bmatrix} 1 & -\theta_{sz} & \theta_{sy} \\ \theta_{sz} & 1 & -\theta_{sx} \\ -\theta_{sy} & \theta_{sx} & 1 \end{bmatrix} \tag{8}$$

Combining Eqs. (6) - (8), and substituting the local coordinate values of the tips into the result, the displacements of the tips can be expressed as follows.

$$x_1 = x_s - \sqrt{3}r_3\theta_{sz}/2 + r_3\theta_{sy}/2 \tag{9}$$

$$x_2 = x_s - r_3\theta_{sy} \tag{10}$$

$$x_3 = x_s + \sqrt{3}r_3\theta_{sz}/2 + r_3\theta_{sy}/2 \tag{11}$$

$$y_1 = y_s - r_3\theta_{sx}/2 \tag{12}$$

$$y_2 = y_s + r_3\theta_{sx} \tag{13}$$

$$y_3 = y_s - r_3\theta_{sx}/2 \tag{14}$$

$$z_1 = z_s + \sqrt{3}r_3\theta_{sx}/2 \tag{15}$$

$$z_2 = z_s \tag{16}$$

$$z_3 = z_s - \sqrt{3}r_3\theta_{sx}/2 \tag{17}$$

2.3. Load-equilibrium conditions

From the free body diagram in Fig. 2, the equilibrium conditions of the motion stage in the deformed configuration can be described:

$$\begin{bmatrix} p \\ f_y \\ f_z \\ m_x \\ m_y \\ m_z \end{bmatrix} = \sum_{i_0=1}^{n=3} \begin{bmatrix} 1 & 0 & 0 & 0 & 0 & 0 \\ 0 & 1 & 0 & 0 & 0 & 0 \\ 0 & 0 & 1 & 0 & 0 & 0 \\ 0 & -z_{i_0}^{''}/\delta & y_{i_0}^{''}/\delta & 1 & 0 & 0 \\ z_{i_0}^{''} & 0 & -x_{i_0}^{''} & 0 & 1 & 0 \\ -y_{i_0}^{''} & x_{i_0}^{''} & 0 & 0 & 0 & 1 \end{bmatrix} \begin{bmatrix} p_{i_0} \\ f_{i_0 y} \\ f_{i_0 z} \\ m_{i_0 x} \\ m_{i_0 y} \\ m_{i_0 z} \end{bmatrix} \tag{18}$$

where $x_{i_0}^{''}$, $y_{i_0}^{''}$ and $z_{i_0}^{''}$ can be obtained from the result of substituting Eq. (8) into Eq. (7).

Neglecting the contribution of rotations in Eq. (18), this simplifies to:

$$p = p_1 + p_2 + p_3 \tag{19}$$

$$f_y = f_{1y} + f_{2y} + f_{3y} \tag{20}$$

$$f_z = f_{1z} + f_{2z} + f_{3z} \tag{21}$$

$$m_y \approx m_{1y} + m_{2y} + m_{3y} + (p_1 + p_3 - 2p_2) r_3/2 \tag{22}$$

$$m_z \approx m_{1z} + m_{2z} + m_{3z} + (p_3 - p_1)\sqrt{3} r_3/2 \tag{23}$$

$$m_x \approx m_{1x} + m_{2x} + m_{3x} + (f_{1z} - f_{3z})\sqrt{3} r_3/(2\delta) + [2f_{2y} - (f_{1y} + f_{3y})] r_3/(2\delta) \tag{24}$$

3. Solution to the nonlinear load-displacement analysis for the three-beam module

The constitutive, compatibility and equilibrium conditions of Sections 2.1 to 2.3 now permit a solution of the nonlinear load-displacement equations in terms of the geometry of the three-beam module. Three methods of increasing accuracy and complexity are presented in this section: an approximate analytical method, an improved analytical method, and a numerical method.

3.1 Approximate analytical solution

An initial FEA showed that, when forces alone are acting, each of two bending angles is approximately two orders of magnitude smaller than its corresponding one of two transverse displacements (θ_{sz} to y_s, θ_{sy} to z_s), and the torsional angle is almost zero. Therefore, the rotational angles are dropped out wherever appropriate below.

a) Solution for θ_{sy} and θ_{sz}

Substituting Eq. (2) into Eq. (22) and again neglecting all the rotational displacements:

$$(p_1 + p_3) - 2p_2 \approx \frac{m_y + (3c + ph) z_s}{r_3/2} \tag{25}$$

Similarly, the substitution of Eq. (1) into Eq. (23) yields

$$(p_3 - p_1) \approx \frac{m_z - (3c + ph) y_s}{\sqrt{3} r_3/2} \tag{26}$$

From Eqs. (9) to (11), one can obtain

$$(x_1 + x_3) - 2x_2 = 3r_3 \sin\theta_{sy} \tag{27}$$

Substituting Eqs. (3) and (12) - (17) into Eq. (27), and substituting Eq. (25) into the result gives the rotational displacement

$$\theta_{sy} \approx \frac{2}{3r_3^2}\left(\frac{1}{d} + y_s^2 r + z_s^2 r\right)[m_y + (3c + ph) z_s] - 2\theta_{sx} y_s i \tag{28}$$

Similarly, the rotational displacement θ_{sz} can also be obtained from Eqs. (9), (11), (3), (12), (14), (15), (17) and (26) as

$$\theta_{sz} = \frac{x_3 - x_1}{\sqrt{3} r_3} \approx \frac{2}{3r_3^2}\left(\frac{1}{d} + y_s^2 r + z_s^2 r\right)[m_z - (3c + ph) y_s] - 2\theta_{sx} z_s i \tag{29}$$

b) Solution for y_s and z_s

Substituting Eq. (1) into Eq. (20) and combining Eqs. (12) - (14), we obtain

$$\begin{aligned} f_y &= f_{1y} + f_{2y} + f_{3y} = ay_1 + c\theta_{sz} + p_1(ey_1 + h\theta_{sz}) + ay_2 + c\theta_{sz} + p_2(ey_2 + h\theta_{sz}) + ay_3 + c\theta_{sz} + p_3(ey_3 + h\theta_{sz}) \\ &= (3a + pe) y_s + (3c + ph)\theta_{sz} + (2p_2 - (p_1 + p_3))\frac{1}{2} r_3 \theta_{sx} e \end{aligned} \tag{30}$$

Rewriting Eq. (30) and replacing θ_{sz} with $-2\theta_{sx} z_s i$ based on Eq. (29), we obtain the transverse translational displacement

$$y_s = \frac{f_y - (3c + ph)(-2\theta_{sx} z_s i) + [(p_1 + p_3) - 2p_2]\frac{1}{2} r_3 \theta_{sx} e}{3a + pe} \tag{31}$$

The transverse translational displacements z_s can be obtained by substituting Eq. (2) into Eq. (21), combining Eqs. (15) - (17) and replacing θ_{sy} with $-2\theta_{sx} y_s i$ based on Eq. (28):

$$z_s = \frac{f_z + (3c + ph)(-2\theta_{sx} y_s i) + (p_3 - p_1)\frac{\sqrt{3}}{2} r_3 \theta_{sx} e}{3a + pe} \tag{32}$$

Finally, substituting Eqs. (25) and (26) into Eqs. (31) and (32), respectively, we obtain the two transverse displacement equations:

$$y_s \approx \frac{f_y - (3c + ph)(-2\theta_{sx} z_s i) + [m_y + (3c + ph) z_s]\theta_{sx} e}{3a + pe} \approx \frac{f_y + m_y \theta_{sx} e}{3a + pe} \tag{33}$$

$$z_s \approx \frac{f_z + (3c + ph)(-2\theta_{sx} y_s i) + [m_z - (3c + ph) y_s]\theta_{sx} e}{3a + pe} \approx \frac{f_z + m_z \theta_{sx} e}{3a + pe} \tag{34}$$

c) Solution for θ_{sx}

Combining Eqs. (1) and (2), and substituting the result along with Eq. (4) into Eq. (24), we have

$$m_x \approx 3\theta_{sx} + 3ar_3^2 \theta_{sx}/\delta + per_3^2 \theta_{sx}/\delta + \frac{\sqrt{3}}{2} r_3 (p_1 - p_3) e z_s/\delta + \frac{1}{2} r_3 [2p_2 - (p_1 + p_3)] e y_s/\delta \tag{35}$$

Substituting Eqs. (25) and (26) into Eq. (35), and substituting Eqs. (33) and (34) into the result, we obtain the torsional angle (rotational displacement):

$$\theta_{sx} \approx \frac{m_x \delta + (m_z f_z + m_y f_y) e/(3a + pe)}{3(\delta + ar_3^2 + \frac{p}{3} er_3^2)} \tag{36}$$

If the torque is normalized by EI/L (rather than by GI_p/L), the torsional angle θ_{sx} becomes

$$\theta_{sx} \approx \frac{m_x + (m_z f_z + m_y f_y) e/(3a + pe)}{3(\delta + ar_3^2 + \frac{p}{3} er_3^2)} \tag{37}$$

d) Solution for x_s

From Eqs. (9) to (11), we have

$$x_s = (x_1 + x_2 + x_3)/3 \tag{38}$$

Substituting Eqs. (3) and (12) - (17) into Eq. (38), substituting Eqs. (25) and (26) into the result and omitting some high order terms of rotational angles, we obtain the axial translational displacement:

$$x_s \approx \frac{p}{3d} + (y_s^2 + z_s^2) i + \frac{p}{3}(y_s^2 + z_s^2) r + r_3^2 \theta_{sx}^2 i + \frac{p}{3} r_3^2 \theta_{sx}^2 r + 2(y_s \theta_{sz} - z_s \theta_{sy}) k - \frac{2}{3}(m_y y_s + m_z z_s)\theta_{sx} r \tag{39}$$

where the terms with $r_3^2\theta_{sx}^2$ are retained since θ_{sx} is the DOF, and they are related to the radius r_3.

In summary, the approximate displacements of the motion stage for a given set of loads are obtained as follows:

(1) Calculate the torsional angle θ_{sx} using Eq. (36) [or Eq. (37)];

(2) Solve for y_s and z_s by substituting the torsional angle into Eqs. (33) and (34);

(3) Calculate θ_{sy} and θ_{sz} by substituting θ_{sx}, y_s and z_s into Eqs. (28) and (29);

(4) Obtain the axial displacement x_s using Eq. (39).

When $m_y f_y = -m_z f_z$, which includes five special cases: $m_y = m_z = 0$; $f_z = f_y = 0$; $m_y = f_z = 0$; $f_y = m_z = 0$; $m_z = -0.5 f_y$ and $m_y = 0.5 f_z$, Eq. (36) simplifies to $\theta_{sx} = m_x\delta/[3(\delta + ar_3^2 + per_3^2/3)]$. This condition holds when the resultant transverse force is perpendicular to the resultant bending moment. In particular, in the case: $m_y = m_z = 0$, the three DOF equations [Eqs. (33), (34) and (36)] are independent, and in the case: $m_z = -0.5 f_y$ and $m_y = 0.5 f_z$, the three rotational angles [Eqs. (28), (29) and (36)] are all equal to zero as long as the axial force $p = 0$ and $m_x = 0$. Furthermore, according to Eqs. (28), (29), (33), (34), (36) and (39), when only a torsional moment is imposed on the motion stage, two of the translational displacements, y_s and z_s, and two of the rotational displacements, θ_{sz} and θ_{sy}, are zero while $\theta_{sx} = m_x\delta/[3(\delta + ar_3^2)]$ and $x_s = r_3^2\theta_{sx}^2 i$ (negative), and this reveals how torsion can reduce the axial displacement x_s. If only the two transverse forces are imposed on the motion stage, the spatial three-beam module can be regarded as a good 2-D translation joint.

It can also be observed from Eqs. (28), (29), (33), (34), (36) and (39) that:

(a) The axial force p affects the transverse displacements (y_s and z_s), which reflects the load-stiffening effect. Either of the two transverse displacement equations shows that the buckling condition $p_{crit1} = -3a/e = -30$ occurs when the transverse stiffness becomes zero. The torsional angle θ_{sx} decreases with increasing (positive) p, which also shows the load-stiffening effect. The torsional angle equation shows a second buckling condition $p_{crit2} = -3(\delta + ar_3^2)/(er_3^2) = -[30 + 3\delta/(er_3^2)]$ when the torsional stiffness becomes zero. Therefore, the buckling load for the spatial three-beam module is $p_{crit} = \max(p_{crit1}, p_{crit2}) = -30$.

(b) The axial displacement x_s has three components: purely elastic effect from the axial force alone, purely kinematic effect such as $(y_s^2 + z_s^2) i + r_3^2 \theta_{sx}^2 i + 2(y_s\theta_{sz} - z_s\theta_{sy}) k$ and elastokinematic effect such as $p(y_s^2 + z_s^2) r/3 + pr_3^2\theta_{sx}^2 r/3 - 2(m_y y_s + m_z z_s)\theta_{sx} r/3$. Similarly, the bending angle, θ_{sy} (θ_{sz}), is also composed of three components.

(c) The torsional angle has a dominant effect on the accuracy of the above equations in comparison with θ_{sz} and θ_{sy}. The smaller $|\theta_{sx}|$ is, the more accurate are the above force-displacement equations.

(d) All the three rotational angles decrease as r_3 increases. For a typical value 0.6 of r_3 and $\theta_{sx} = 0$, θ_{sz} and θ_{sy} can be in the order of 1×10^{-4} if $d = 40000$ (i.e. $L/D_0 = 50$). This reveals the fact that the essence of constraint-based design is a combination of the effects of large values of d and small values of r. Furthermore, if θ_{sx} and y_s (or z_s) are all relatively large in absolute value, θ_{sy} (θ_{sz}) is affected by purely kinematic effect: $-2\theta_{sx} y_s i$ (or $-2\theta_{sx} z_s i$) dominantly.

(e) The translational displacement, y_s (or z_s), is weakly dependent on m_x, m_y, m_z, p and f_z (or f_y) (Maxwell Reciprocity [5,

24]), and strongly dependent on f_y (or f_z). Here, f_y (or f_z) is a dominant load in determining y_s (or z_s), whereas m_z, m_x, m_y, p and f_z (or f_y) are non-dominant loads. Furthermore, torsional angle θ_{sx} is weakly dependent on m_y, m_z, f_y, f_z and p, and strongly dependent on m_x (m_x is a dominant load in determining θ_{sx}).

3.2 Improved analytical method

For relatively large absolute values of θ_{sx} (even including θ_{sy} or θ_{sz}), the dependence of a transverse translational displacement on the relevant non-dominant loads becomes significant, particularly if the absolute values of the relevant dominant load are small relative to the non-dominant ones. Moreover, the purely kinematic effect and the elastokinematic effect in Eq. (4), the second-order terms in rotational angles neglected in the product of the three rotation matrices in Eq. (8), and the rotation contributions in Eq. (18) need also to be retained wherever appropriate. In addition, we may approximate θ_{sy} and θ_{sz} using Eqs. (28) and (29), respectively, in the appropriate derivation below.

Using Eq. (18), Eqs (22) - (24) for the moment-equilibrium conditions after deformation can be rewritten as

$$m_y \approx m_{1y} + m_{2y} + m_{3y} + (p_1 + p_3 - 2p_2)\frac{r_3}{2} + (p_1 - p_3)\frac{\sqrt{3}}{2}r_3\theta_{sx} + [2f_{2z} - (f_{1z} + f_{3z})]\frac{1}{2}r_3\theta_{sy} + (f_{1z} - f_{3z})\frac{\sqrt{3}}{2}r_3\theta_{sz} \quad (40a)$$

$$m_z \approx m_{1z} + m_{2z} + m_{3z} + (p_3 - p_1)\frac{\sqrt{3}}{2}r_3 + [(p_1 + p_3) - 2p_2]\frac{r_3}{2}\theta_{sx} + (f_{3y} - f_{1y})\frac{\sqrt{3}}{2}r_3\theta_{sz} + [(f_{1y} + f_{3y}) - 2f_{2y}]\frac{1}{2}r_3\theta_{sy} \quad (40b)$$

$$m_x\delta \approx \delta(m_{1x} + m_{2x} + m_{3x}) + (f_{1z} - f_{3z})\frac{\sqrt{3}}{2}r_3 + [2f_{2y} - (f_{1y} + f_{3y})]\frac{1}{2}r_3 + (f_{3y} - f_{1y})\frac{\sqrt{3}}{2}r_3\theta_{sx} + [2f_{2z} - (f_{1z} + f_{3z})]\frac{1}{2}r_3\theta_{sx} \quad (40c)$$

From Eqs. (1), (2) and (12) - (17), one can obtain

$$f_{1z} - f_{3z} = \sqrt{3}ar_3\theta_{sx} + (p_1 - p_3)(ez_s - h\theta_{sy}) + (p_1 + p_3)e\sqrt{3}r_3\theta_{sx}/2 \quad (41a)$$

$$2f_{2y} - (f_{1y} + f_{3y}) = 3ar_3\theta_{sx} + [2p_2 - (p_1 + p_3)](ey_s + h\theta_{sz}) + [4p_2 + (p_1 + p_3)]er_3\theta_{sx}/2 \quad (41b)$$

$$f_{3y} - f_{1y} = (p_3 - p_1)(ey_s + h\theta_{sz}) + (p_1 - p_3)er_3\theta_{sx}/2 \quad (41c)$$

$$2f_{2z} - (f_{1z} + f_{3z}) = [2p_2 - (p_1 + p_3)](ez_s - h\theta_{sy}) + (p_3 - p_1)e\sqrt{3}r_3\theta_{sx}/2 \quad (41d)$$

where p_1+p_3 and $4p_2$+(p_1+p_3) can also be represented by [2p+(p_1+p_3-2p_2)]/3 and 2p-(p_1+p_3-2p_2), respectively.

Retaining the bending angles in Eqs. (31) and (32), the two transverse displacements are obtained as

$$y_s = \frac{f_y - (3c + ph)\theta_{sz} + [(p_1 + p_3) - 2p_2]\frac{1}{2}r_3\theta_{sx}e}{3a + pe} \quad (42)$$

$$z_s = \frac{f_z + (3c + ph)\theta_{sy} + (p_3 - p_1)\frac{\sqrt{3}}{2}r_3\theta_{sx}e}{3a + pe} \quad (43)$$

where accurate solutions for (p_1+p_3)-2p_2 and p_3-p_1 can be obtained by substituting Eq. (41) into Eqs. (40a) and (40b) and combining the results with Eqs. (1), (2) and (12)-(17):

$$\begin{aligned}(p_1 + p_3) - 2p_2 &= \frac{m_y + [(3c + ph)z_s - (3b + pg)\theta_{sy}] - \{m_z - [(3c + ph)y_s + (3b + pg)\theta_{sz}]\}\theta_{sx}(h-1) - (3a + pe)r_3^2\theta_{sz}\theta_{sx}/2}{(r_3/2)(\theta_{sx}^2(h-1)^2 + 1)} \\ &\approx \frac{m_y + [(3c + ph)z_s - (3b + pg)\theta_{sy}] - [m_z - (3c + ph)y_s]\theta_{sx}(h-1)}{(r_3/2)}\end{aligned} \quad (44)$$

$$\begin{aligned}p_3 - p_1 &= \frac{m_z - [(3c + ph)y_s + (3b + pg)\theta_{sz}] + \{m_y + [(3c + ph)z_s - (3b + pg)\theta_{sy}]\}\theta_{sx}(h-1) + (3a + pe)r_3^2\theta_{sy}\theta_{sx}/2}{(\sqrt{3}r_3/2)(\theta_{sx}^2(h-1)^2 + 1)} \\ &\approx \frac{m_z - [(3c + ph)y_s + (3b + pg)\theta_{sz}] + [m_y + (3c + ph)z_s]\theta_{sx}(h-1)}{(\sqrt{3}r_3/2)}\end{aligned} \quad (45)$$

For relatively large absolute values of θ_{sx}, Eq. (28) is re-written as

$$\begin{aligned}3r_3\theta_{sy} &= (x_1 + x_3) - 2x_2 - 3r_3\theta_{sx}\theta_{sz} \\ &\approx \frac{(p_3 + p_1) - 2p_2}{d} + [(y_1^2 + y_3^2) - 2y_2^2]i + [(z_1^2 + z_3^2) - 2z_2^2]i + 2k\theta_{sz}(y_1 + y_3 - 2y_2) - 2k\theta_{sy}(z_1 + z_3 - 2z_2) + [(p_1y_1^2 + p_3y_3^2) - 2p_2y_2^2]r \\ &+ [(p_1z_1^2 + p_3z_3^2) - 2p_2z_2^2]r + 2[(p_1 + p_3) - 2p_2](y_s\theta_{sz} - z_s\theta_{sy})q - 3r_3\theta_{sx}\theta_{sz} \\ &\approx \frac{(p_3 + p_1) - 2p_2}{d} - 6r_3\theta_{sx}y_si - 6r_3\theta_{sx}\theta_{sz}(k + 0.5) + [(p_1 + p_3) - 2p_2](y_s^2 + z_s^2)r - [(p_1 + p_3) + 4p_2]r_3\theta_{sx}y_sr + (p_1 - p_3)\sqrt{3}r_3\theta_{sx}z_sr + [(p_1 + p_3) - 2p_2]r_3^2\theta_{sx}^2r \\ &- 4[(p_1 + p_3) - 2p_2](y_sz_s - z_sy_s)\theta_{sx}iq \\ &\approx \frac{(p_3 + p_1) - 2p_2}{d} - 6r_3\theta_{sx}y_si - 3r_3\theta_{sx}\theta_{sz} + [(p_1 + p_3) - 2p_2](y_s^2 + z_s^2)r + [((p_1 + p_3) - 2p_2) - 2p]r_3\theta_{sx}y_sr + (p_1 - p_3)\sqrt{3}r_3\theta_{sx}z_sr + [(p_1 + p_3) - 2p_2]r_3^2\theta_{sx}^2r\end{aligned} \quad (46)$$

The substitution of Eqs. (29), (44) and (45) into Eq. (46) produces

$$\begin{aligned}\theta_{sy} \approx{}& \frac{2}{3r_3^2}\left[\frac{1}{d} + (y_s^2 + z_s^2 + r_3^2\theta_{sx}^2)r\right][m_y + (3c + ph)z_s - m_z\theta_{sx}(h-1)] \\ &- \frac{2}{3r_3^2}\left[\frac{1}{d} + (y_s^2 + z_s^2 + r_3z_s)r\right][m_z + m_y\theta_{sx}(h-1)]\theta_{sx} - 2\theta_{sx}y_s\left(i + \frac{p}{3}r\right) + 2\theta_{sx}^2z_si\end{aligned} \quad (47)$$

Similarly, Eq. (29) is re-written as

$$\begin{aligned}
&\sqrt{3}r_3\theta_{sz} = x_3 - x_1 + \sqrt{3}r_3\theta_{sx}\theta_{sy} \\
&\approx \frac{(p_3-p_1)}{d} + (y_3^2 - y_1^2)i + (z_3^2 - z_1^2)i + 2k\theta_{sz}(y_3 - y_1) - 2k\theta_{sy}(z_3 - z_1) + (p_3 y_3^2 - p_1 y_1^2)r + (p_3 z_3^2 - p_1 z_1^2)r + 2(p_3 - p_1)(y_s\theta_{sz} - z_s\theta_{sy})q + \sqrt{3}r_3\theta_{sx}\theta_{sy} \\
&\approx \frac{(p_3-p_1)}{d} - 2\sqrt{3}r_3\theta_{sx}z_s i + 2\sqrt{3}r_3\theta_{sx}\theta_{sy}(k+0.5) + (p_3-p_1)(y_s^2+z_s^2)r + (p_1-p_3)r_3\theta_{sx}y_s r - (p_1+p_3)\sqrt{3}r_3\theta_{sx}z_s r + (p_3-p_1)r_3^2\theta_{sx}^2 r - 4(p_3-p_1)(y_s z_s - z_s y_s)\theta_{sx} iq \\
&\approx \frac{(p_3-p_1)}{d} - 2\sqrt{3}r_3\theta_{sx}z_s i + \sqrt{3}r_3\theta_{sx}\theta_{sy} + (p_3-p_1)(y_s^2+z_s^2)r + (p_1-p_3)r_3\theta_{sx}y_s r - \frac{2p+[(p_1+p_3)-2p_2]}{3}\sqrt{3}r_3\theta_{sx}z_s r + (p_3-p_1)r_3^2\theta_{sx}^2 r
\end{aligned} \tag{48}$$

Substituting Eqs. (28), (44) and (45) into Eq. (48), we have

$$\begin{aligned}
\theta_{sz} \approx{}& \frac{2}{3r_3^2}\left[\frac{1}{d} + (y_s^2 + z_s^2 + r_3^2\theta_{sx}^2 - r_3\theta_{sx}y_s)r\right][m_z - (3c+ph)y_s + m_y\theta_{sx}(h-1)] \\
&+ \frac{2}{3r_3^2}\left[\frac{1}{d} + (y_s^2 + z_s^2)r\right][m_y + m_z\theta_{sx}(h-1)]\theta_{sx} - 2\theta_{sx}z_s(i + \frac{p}{3}r) - 2\theta_{sx}^2 y_s i
\end{aligned} \tag{49}$$

Then, substituting Eqs. (44) and (45) into Eqs. (42) and (43), respectively, the two transverse displacements can be obtained as

$$y_s \approx \frac{f_y - (3c+ph)\theta_{sz} + \{m_y + [(3c+ph)z_s - (3b+pg)\theta_{sy}] - [m_z - (3c+ph)y_s]\theta_{sx}(h-1)\}\theta_{sx}e}{3a+pe} \tag{50}$$

$$z_s \approx \frac{f_z + (3c+ph)\theta_{sy} + \{m_z - [(3c+ph)y_s + (3b+pg)\theta_{sz}] + [m_y + (3c+ph)z_s]\theta_{sx}(h-1)\}\theta_{sx}e}{3a+pe} \tag{51}$$

Equations (50) and (51) can be further simplified as

$$y_s \approx \frac{f_y - (3c+ph)(\bar{\theta}_{sz} - 2\theta_{sx}z_s i) + [m_y + (3c+ph)z_s]\theta_{sx}e - m_z\theta_{sx}^2(h-1)e}{3a+pe} \approx \bar{y}_s - \frac{(3c+ph)\bar{\theta}_{sz} + m_z\theta_{sx}^2(h-1)e}{3a+pe} \tag{52}$$

$$z_s \approx \frac{f_z + (3c+ph)(\bar{\theta}_{sy} - 2\theta_{sx}y_s i) + [m_z - (3c+ph)y_s]\theta_{sx}e + m_y\theta_{sx}^2(h-1)e}{3a+pe} \approx \bar{z}_s + \frac{(3c+ph)\bar{\theta}_{sy} + m_y\theta_{sx}^2(h-1)e}{3a+pe} \tag{53}$$

where $\bar{\theta}_{sz} = \frac{2}{3r_3^2}\left[\frac{1}{d} + (\bar{y}_s^2 + \bar{z}_s^2)r\right][m_z - (3c+ph)\bar{y}_s]$, $\bar{\theta}_{sy} = \frac{2}{3r_3^2}\left[\frac{1}{d} + (\bar{y}_s^2 + \bar{z}_s^2)r\right][m_y + (3c+ph)\bar{z}_s]$, $\bar{y}_s = \frac{f_y + m_y\theta_{sx}e}{3a+pe}$, $\bar{z}_s = \frac{f_z + m_z\theta_{sx}e}{3a+pe}$.

Substituting Eq. (41) into Eq. (40c) and combining with Eq. (4), we have

$$\begin{aligned}
m_x\delta \approx{}& 3\delta\theta_{sx} + 3c(\theta_{sz}z_s + \theta_{sy}y_s) + ph(\theta_{sz}z_s + \theta_{sy}y_s) + 3ar_3^2\theta_{sx} + per_3^2\theta_{sx} \\
&+ \frac{\sqrt{3}}{2}r_3(p_1 - p_3)[(ez_s - h\theta_{sy}) - (ey_s + h\theta_{sz})\theta_{sx}] + \frac{1}{2}r_3[2p_2 - (p_1 + p_3)][(ey_s + h\theta_{sz}) + (ez_s - h\theta_{sy})\theta_{sx}]
\end{aligned} \tag{54}$$

We can further substitute Eqs. (44), (45), (47), (49), (52) and (53) into Eq. (54) and omit some high order terms of rotational angles. Then we simplify the torsional angle as follows:

$$\begin{aligned}
\theta_{sx} \approx{}& \{m_x\delta + [m_z - (3c+ph)\hat{y}_s - (3b+pg)(\bar{\theta}_{sz} - 2\theta_{sx}\hat{z}_s i) + [m_y + (3c+ph)\hat{z}_s]\theta_{sx}(h-1)][(e\hat{z}_s - h\bar{\theta}_{sy} + 2h\theta_{sx}\hat{y}_s i) - e\hat{y}_s\theta_{sx}] \\
&+ [m_y + (3c+ph)\hat{z}_s - (3b+pg)(\bar{\theta}_{sy} - 2\theta_{sx}\hat{y}_s i) - [m_z - (3c+ph)\hat{y}_s]\theta_{sx}(h-1)][(e\hat{y}_s + h\bar{\theta}_{sz} - 2h\theta_{sx}\hat{z}_s i) + e\hat{z}_s\theta_{sx}] \\
&- (3c+ph)(\bar{\theta}_{sz}\hat{z}_s + \bar{\theta}_{sy}\hat{y}_s)\}/\{3[\delta + ar_3^2 + \frac{p}{3}er_3^2 - 2ci(\hat{z}_s^2 + \hat{y}_s^2) - \frac{2phi}{3}(\hat{z}_s^2 + \hat{y}_s^2)]\}
\end{aligned} \tag{55}$$

where $\hat{y}_s = \frac{f_y + m_y\theta_{sx}e - (3c+ph)\bar{\theta}_{sz}}{3a+pe}$, $\hat{z}_s = \frac{f_z + m_z\theta_{sx}e + (3c+ph)\bar{\theta}_{sy}}{3a+pe}$. Only one real solution is the desired solution for the equation with one unknown θ_{sx}. Equation (55) can be shown to reduce to Eq. (36) for relatively small $|\theta_{sx}|$.

In addition, substituting the torsional angle θ_{sx} obtained from Eq. (55) into Eqs. (52) and (53), the two transverse displacements, y_s and z_s, can be found.

Once θ_{sx}, y_s and z_s have been obtained, the other two rotational angles, θ_{sy} and θ_{sz}, can be obtained using Eqs. (47) and (49), and the axial displacement x_s can then be obtained using Eqs. (3) and (9) - (17) as

$$\begin{aligned}
x_s = \frac{1}{3}(x_1 + x_2 + x_3) \approx{}& \frac{p}{3d} + (y_s^2 + z_s^2)i + \frac{p}{3}(y_s^2 + z_s^2)r + r_3^2\theta_{sx}^2 i + \frac{p}{3}r_3^2\theta_{sx}^2 r + \frac{1}{3}[(2p_2 - (p_1 + p_3))r_3 y_s + (p_1 - p_3)\sqrt{3}r_3 z_s]\theta_{sx}r \\
&+ 2(y_s\theta_{sz} - z_s\theta_{sy})k + (\theta_{sz}^2 + \theta_{sy}^2)j + \frac{2}{3}p(y_s\theta_{sz} - z_s\theta_{sy})q + \frac{1}{3}[(2p_2 - (p_1 + p_3))r_3\theta_{sz} - (p_1 - p_3)\sqrt{3}r_3\theta_{sy}]\theta_{sx}q + \frac{p}{3}(\theta_{sz}^2 + \theta_{sy}^2)s
\end{aligned} \tag{56}$$

Substituting Eqs. (44) and (45) into Eq. (56) and making further simplification, we have

$$\begin{aligned}
x_s \approx{}& \frac{p}{3d} + (y_s^2 + z_s^2)i + \frac{p}{3}(y_s^2 + z_s^2)r + r_3^2\theta_{sx}^2 i + \frac{p}{3}r_3^2\theta_{sx}^2 r + 2(y_s\theta_{sz} - z_s\theta_{sy})k - \frac{2}{3}(m_y y_s + m_z z_s)\theta_{sx}r \\
&- \frac{2}{3}[(m_y + (3c+ph)z_s)\theta_{sz} - (m_z - (3c+ph)y_s)\theta_{sy}]\theta_{sx}q
\end{aligned} \tag{57}$$

Equations (47), (49), (52), (53), (55) and (57) are the improved analytical load-displacement equations for large $|\theta_{sx}|$, which can capture more nonlinear effects. It can be shown that $\theta_{sx} \approx 0$ for the five special loading cases: $m_x = m_y = m_z = 0$; $m_x = f_z = f_y = 0$; $m_x = m_y = f_z = 0$; $m_x = f_y = m_z = 0$; $m_x = 0$, $m_z = -0.5f_y$ and $m_y = 0.5f_z$.

If m_y or m_z in Eqs. (52) and (53) and all of the dominant transverse forces are very small in absolute value, we can obtain more accurate solutions to the load-displacement equations. Starting from the θ_{sx}, θ_{sy} and θ_{sz} obtained above, the two accurate transverse displacements (y_s and z_s) can be obtained from Eqs. (50) and (51). Then, we can obtain more accurate values of θ_{sx},

θ_{sy}, θ_{sz} and x_s step-by-step by substituting the above y_s and z_s into Eqs. (55), (47), (49) and (57).

3.3 Numerical method

Exact solutions for the nonlinear load-displacement equations can be obtained numerically without the need for approximation, although this has the disadvantage that the qualitative behavior of the CPMs is more difficult to explore.

The numerical scheme involves seven unknown terms: (p_1+p_3)-$2p_2$, p_3-p_1, θ_{sx}, θ_{sy}, θ_{sz}, y_s and z_s that are obtained by solving the seven following equations, obtained from Eqs. (42)-(46), (48) and (54):

$$y_s = \{f_y - (3c+ph)\theta_{sz} + [(p_1+p_3)-2p_2]\frac{1}{2}r_3\theta_{sx}e\}/(3a+pe) \tag{58}$$

$$z_s = \{f_z + (3c+ph)\theta_{sy} + (p_3-p_1)\frac{\sqrt{3}}{2}r_3\theta_{sx}e\}/(3a+pe) \tag{59}$$

$$(p_1+p_3)-2p_2 = \frac{m_y + [(3c+ph)z_s - (3b+pg)\theta_{sy}] - \{m_z - [(3c+ph)y_s + (3b+pg)\theta_{sz}]\}\theta_{sx}(h-1) - (3a+pe)r_3^2\theta_{sz}\theta_{sx}/2}{(r_3/2)} \tag{60}$$

$$p_3-p_1 = \frac{m_z - [(3c+ph)y_s + (3b+pg)\theta_{sz}] + \{m_y + [(3c+ph)z_s - (3b+pg)\theta_{sy}]\}\theta_{sx}(h-1) + (3a+pe)r_3^2\theta_{sy}\theta_{sx}/2}{(\sqrt{3}r_3/2)} \tag{61}$$

$$\begin{aligned} 3r_3\theta_{sy} &= \frac{(p_3+p_1)-2p_2}{d} - 6r_3\theta_{sx}y_s i - 6r_3\theta_{sx}\theta_{sz}(k+0.5) + [(p_1+p_3)-2p_2](y_s^2+z_s^2)r \\ &+ [((p_1+p_3)-2p_2)-2p]r_3\theta_{sx}y_s r + (p_1-p_3)\sqrt{3}r_3\theta_{sx}z_s r + [(p_1+p_3)-2p_2]r_3^2\theta_{sx}^2 r + 2[(p_1+p_3)-2p_2](y_s\theta_{sz}-z_s\theta_{sy})q \end{aligned} \tag{62}$$

$$\begin{aligned} \sqrt{3}r_3\theta_{sz} &= \frac{(p_3-p_1)}{d} - 2\sqrt{3}r_3\theta_{sx}z_s i + 2\sqrt{3}r_3\theta_{sx}\theta_{sy}(k+0.5) + (p_3-p_1)(y_s^2+z_s^2)r \\ &+ (p_1-p_3)r_3\theta_{sx}y_s r - \frac{2p+[(p_1+p_3)-2p_2]}{3}\sqrt{3}r_3\theta_{sx}z_s r + (p_3-p_1)r_3^2\theta_{sx}^2 r + 2(p_3-p_1)(y_s\theta_{sz}-z_s\theta_{sy})q \end{aligned} \tag{63}$$

$$\begin{aligned} m_x\delta &= 3\delta\theta_{sx} + (3c+ph)(\theta_{sz}z_s + \theta_{sy}y_s) + (3a+pe)r_3^2\theta_{sx} \\ &+ \frac{\sqrt{3}}{2}r_3(p_1-p_3)[(ez_s - h\theta_{sy}) - (ey_s + h\theta_{sz})\theta_{sx}] + \frac{1}{2}r_3[2p_2-(p_1+p_3)][(ey_s+h\theta_{sz}) + (ez_s - h\theta_{sy})\theta_{sx}] \end{aligned} \tag{64}$$

Once (p_1+p_3)-$2p_2$, p_3-p_1, θ_{sx}, θ_{sy}, θ_{sz}, y_s and z_s have been obtained using Maple *fsolve* function, they can be substituted into Eq. (56) to obtain the axial displacement x_s. We can also obtain p_1 and p_2 and p_3 by combining Eqs. (60), (61) and (19), which is useful for further stress analysis.

3.4. Discussion

a) Validity condition of the proposed approaches

The proposed models are valid only for small deflections (usually all normalized displacements less than 0.1 [5]) and large ratios of length to diameter, i.e. slenderness ratios (usually L/D_0 more than 10 [38] for slender beams ignoring shear deformation). If the proposed nonlinear models are applied to the analysis of CPMs under the conditions of large deflections or small slenderness ratios (for Timoshenko beams), errors between the analytical results and real results will be unacceptable, but these models can still capture certain nonlinear constraint characteristics of the CPMs.

Let us now discuss the range of r_3 under given conditions. If we make a rotational angle (such as θ_{sz}) smaller than α times (usually ≥ 50) a corresponding transverse displacement (such as y_s) in absolute value under only one transverse force acting (such as f_y), we have the following relationship based on Eq. (29):

$$\frac{2}{3r_3^2}(1/d + y_s^2 r)(-3cy_s) \leq y_s/\alpha$$

The above equation is simplified to determine the range of r_3:

$$r_3^2 \geq 12\alpha/d$$

b) Extensible application of the proposed approaches to CPMs with regular polygon cross-section beams and varying-thickness beams

It should be noted that the above normalized and nonlinear models are also applicable for the CPMs with regular polygon cross-section beams (ignoring warping effect under torsion), but the non-dimensional coefficient d should be modified accordingly. For example, for the square cross-section multi-beam module, $d=12/(T/L)^2$ (T is the thickness of the beam). Moreover, these models can be used to deal with generalized beam modules by modifying the coefficients a, b, c, d, e, g, h, i, j, k, q, r and s based on Ref. [23], and using $\delta=G/(Ea_0)$ and then replacing $m_x\delta$ with $2a_0m_x\delta$ in Eqs. (36), (55) and (64). The generalized beam, with the same overall beam length L, is composed of two uniform compliant segments (each normalized length is a_0) and one rigid segment.

c) Characteristics of three approaches

In order to illustrate the applicability of the various solutions, an example three-beam CPM is analyzed below. The CPM is taken to be made from an aluminum alloy for which Young's modulus, E, is 69,000 Nmm^{-2} and Poisson's ratio, v, is 0.33. The dimensions are D_0=4 mm (d=2500), R_3=30 mm (r_3=0.6) and L=50 mm. All the normalized external transverse forces need to be approximately over [-3.6, 3.6] yielding normalized transverse displacements over [-0.1, 0.1] as shown in Fig. 5.

The normalized external torque needs to be approximately in the order of 1.8 to limit the torsional angle to the order of 0.1. Other normalized external loads may be all of order of 1.8 or greater compared with the pre-determined loads.

In practice, the simpler and more analytical the approach is, the more useful the analysis for design of CPMs is. If each of the dominate forces for transverse displacements, such as f_y for y_s, is relatively large (for example, 2 times larger than all the relevant non-dominant moments in absolute value) or two bending moments are both zero (m_y=m_z=0), the approximate analytical solution should be acceptable for design purposes (the case under the latter condition is shown in Fig. 3). When the above condition does not hold, a balance needs to be made between accuracy and complexity.

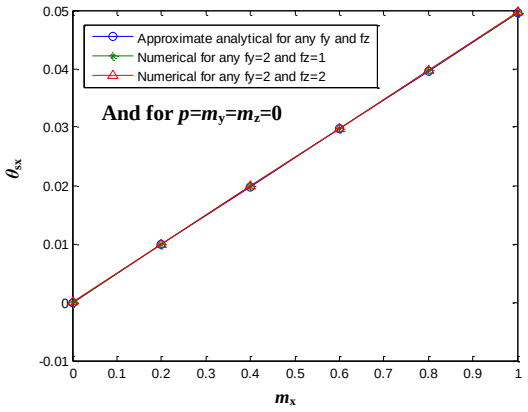

Fig. 3 Comparison of results obtained using three approaches (case with no bending moments acting).

Table 1 shows the calculated displacements of the motion stage of the three-beam module for the approximate and improved analytical models and for the numerical model under loads: f_z=2, m_z=10 ($m_z f_z$ =20) and p=m_x=m_y=m_z=0, i.e. where the torsional angle is relatively large.

Table 1
Comparison of the results obtained using the three nonlinear methods under the large torsion

Displacements / Method	y_s	z_s	x_s	θ_{sz}	θ_{sy}	θ_{sx}
Approximate analytical method	0.00	0.0702	-0.00390	0.0112	-9.518×10^{-4}	0.0438
Improved analytical method	0.00513	0.0755	-0.00424	0.0131	-1.106×10^{-3}	0.0607
Numerical method	0.00514	0.0764	-0.00436	0.0131	-1.111×10^{-3}	0.0609
Error between improved and approximate analytical methods	100%	7.02 %	7.80%	14.50%	13.94%	28.08%

We can observe from Table 1 that, for relatively large θ_{sx}, the error (|(improved analytical result - approximated analytical result)/improved analytical result|×100%) is relatively large and is unacceptably high for y_s since the dominant load f_y for y_s is zero. Table 1 also shows that the approximations for the improved analytical method are reasonable, leading to very small differences between the analytical and numerical solutions. If the loading is changed to f_z=2, m_z=5 ($m_z f_z$=10), and p=m_x=m_y =m_z =0, the error in the torsional angle reduces from the 28.08% in Tab. 1 to 6.40%.

Figure 4 shows that the torsional angle error between the improved and approximate analytical (or numerical) methods increases at an accelerating rate as the ratio of f_z to m_z decreases starting at around 1.6, and also verifies the accuracy of the improved analytical method. It is concluded that the difference between the solutions obtained using these two methods decreases with the increase of the transverse loads.

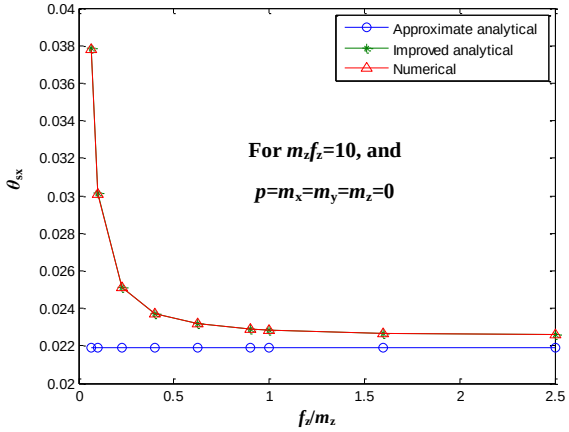

Fig. 4 Comparison for fixed product of $m_z f_z$.

d) Linear analytical approaches

If the effects of load-stiffening and elastokinematic non-linearities in Eqs. (1) - (4) are all neglected, the linear load-

displacement equations of the tip of the i_0-th beam are:

$$\begin{cases} \begin{bmatrix} f_{i_0 y} \\ m_{i_0 z} \end{bmatrix} = \begin{bmatrix} a & c \\ c & b \end{bmatrix} \begin{bmatrix} y_{i_0} \\ \theta_{i_0 z} \end{bmatrix} \\ \begin{bmatrix} f_{i_0 z} \\ -m_{i_0 y} \end{bmatrix} = \begin{bmatrix} a & c \\ c & b \end{bmatrix} \begin{bmatrix} z_{i_0} \\ -\theta_{i_0 y} \end{bmatrix} \\ x_{i_0} = \dfrac{1}{d} p_{i_0} + [y_{i_0}, \theta_{i_0 z}] \begin{bmatrix} i & k \\ k & j \end{bmatrix} \begin{bmatrix} y_{i_0} \\ \theta_{i_0 z} \end{bmatrix} + [z_{i_0}, -\theta_{i_0 y}] \begin{bmatrix} i & k \\ k & j \end{bmatrix} \begin{bmatrix} z_{i_0} \\ -\theta_{i_0 y} \end{bmatrix} \\ \theta_{i_0 x} = m_{i_0 x} - c(\theta_{i_0 z} z_{i_0} + \theta_{i_0 y} y_{i_0}) / \delta \end{cases} \tag{65}$$

Using Eq. (65), and following the solution process in section 3.1, one can obtain the linear load-displacement equations of the motion stage as

$$\begin{cases} \theta_{sx} \approx \dfrac{m_x \delta}{3(\delta + a r_3^2)}; \quad \theta_{sy} \approx \dfrac{2}{3 r_3^2 d}(m_y + 3c\bar{z}_s) - 2\theta_{sx}\bar{y}_s i; \quad \theta_{sz} \approx \dfrac{2}{3 r_3^2 d}(m_z - 3c\bar{y}_s) - 2\theta_{sx}\bar{z}_s i \\ y_s \approx \dfrac{f_y - (3c + ph)\theta_{sz}}{3a}; \quad z_s \approx \dfrac{f_z + (3c + ph)\theta_{sy}}{3a} \\ x_s \approx \dfrac{p}{3d} + y_s^2 i + z_s^2 i + r_3^2 \theta_{sx}^2 i + 2(y_s \theta_{sz} - z_s \theta_{sy}) k \end{cases} \tag{66}$$

where $\bar{y}_s = f_y / 3a$, $\bar{z}_s = f_z / 3a$.

Figures 5-7 show a comparison of results using linear and nonlinear approximate analytical analysis for $m_x = m_y = m_z = 0$ (in which case, θ_{sx}=0). Figure 7 also shows that Eq. (66) only captures the effects of dominant loads (such as m_z, f_y) upon the rotational displacements (like θ_{sz}) while the nonlinear equation [Eq. (29)] captures the effects of all loads upon the rotational displacements. Thus, the linear equations may be applicable under a very small range of deflection, such as that indicated by the rectangular area in Fig. 7 drawn for 1.65% error compared with the nonlinear analysis.

If the purely kinematic component in Eq. (3) is also neglected, the single beam load-displacement equations are simplified and the approximate linear load-displacement equations of the motion stage, similar to the ones used in [29-30], can be derived (see Ref. [32] for details).

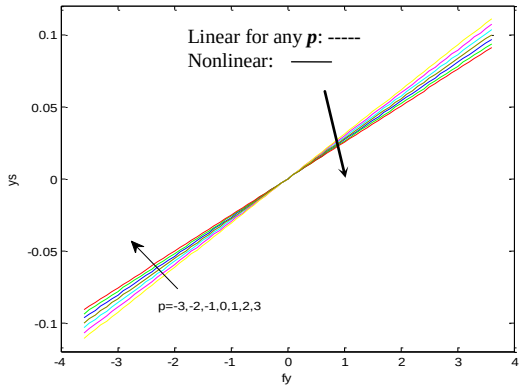

Fig. 5 Primary stiffness in the Y direction.

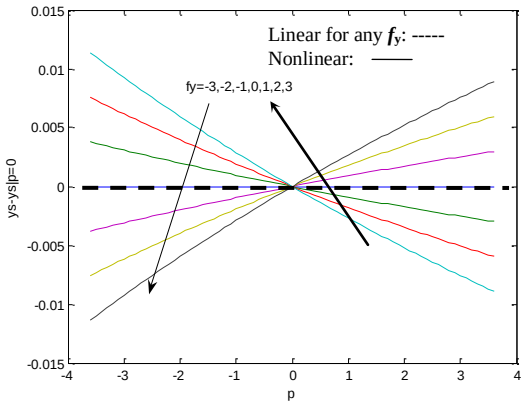

Fig. 6 Cross-axis error.

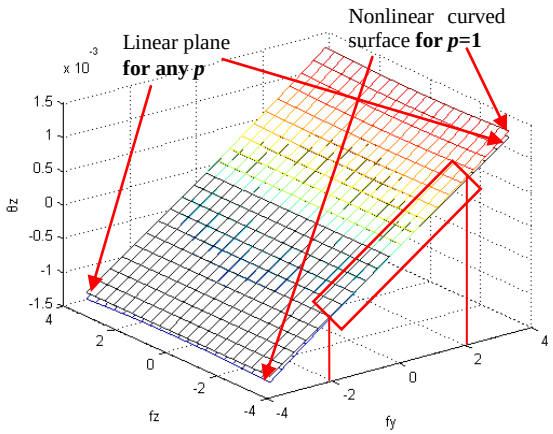

Fig. 7 Rotational angle about the Z-axis.

4. FEA verification for the three-beam module

The displacements obtained for the example CPM using FEA with Comsol large-deformation analysis are compared with the three nonlinear methods in Tab. 2. The FEA translational displacements were given directly by the software, and the rotational angles were calculated from the displacements of points o_1, o_2, and o_3 using Eqs. (9), (10) and (13). The other nonlinear results were obtained by first normalizing the loads then substituting these into the analytical equations correspondingly to obtain the normalized translational displacements and the actual rotational angles (in radians). The actual translational displacements (in mm) were then obtained by multiplying the normalized translational displacements by L.

Table 2 shows that the displacement errors (|(analytical result - FEA result)/analytical result|×100%) between FEA method and any of the three analytical nonlinear methods are within 3.5% and considerably less for θ_{sx} (|analytical result - FEA result|). Here, the bold data are the normalized translational displacements. As mentioned earlier, it can be observed from Tab. 2 that the two bending angles, θ_{sz} and θ_{sy}, are approximately two orders smaller than the normalized transverse translational displacements, y_s and z_s, respectively, and the torsional angle, θ_{sx}, is 3.33×10^{-6} small.

Figures 8-11 show more results obtained using both the FEA and the approximate analytical equations [Eqs. (28), (29), (33), (34), (36) and (39)] without moments acting. It can be seen from these figures that the average errors between the analytical results and FEA results for a given force are acceptable. This verifies the accuracy of the proposed nonlinear equations for the spatial three-beam module.

Table 2
Results contrast between FEA and analytical analysis for P=10N, F_z=10N, F_y=249.59N, M_x=M_y=M_z=0

Displacements / Method	Y_s (mm)	y_s	Z_s (mm)	z_s	X_s (mm)	x_s	θ_{sz} (radian)	θ_{sy} (radian)	θ_{sx} (radian)
FEA method	1.0050	**0.02010**	0.0403	**8.0534×10^{-4}**	-0.0120	**-2.3958×10^{-4}**	2.5980×10^{-4}	-1.0802×10^{-5}	3.3333×10^{-6}
Approximate analytical method	0.9985	**0.01998**	0.0400	**8.0000×10^{-4}**	-0.0120	**-2.3958×10^{-4}**	2.6690×10^{-4}	-1.0682×10^{-5}	0
Improved analytical method	1.0050	**0.02012**	0.0403	**8.0534×10^{-4}**	-0.0121	**-2.4279×10^{-4}**	2.6869×10^{-4}	-1.0753×10^{-5}	6.5715×10^{-15}
Numerical method	1.0050	**0.02012**	0.0403	**8.0533×10^{-4}**	-0.0121	**-2.4280×10^{-4}**	2.6631×10^{-4}	-1.0658×10^{-5}	-2.8988×10^{-15}
Error between approximate analytical method and FEA	0.65 %		0.74 %		0.00 %		2.66%	1.10 %	3.3333×10^{-6}
Error between improved analytical method and FEA	0.00%		0.00 %		0.82 %		3.30%	0.65 %	3.3333×10^{-6}
Error between numerical method and FEA	0.00 %		0.00 %		0.82 %		2.44%	2.87 %	3.3333×10^{-6}

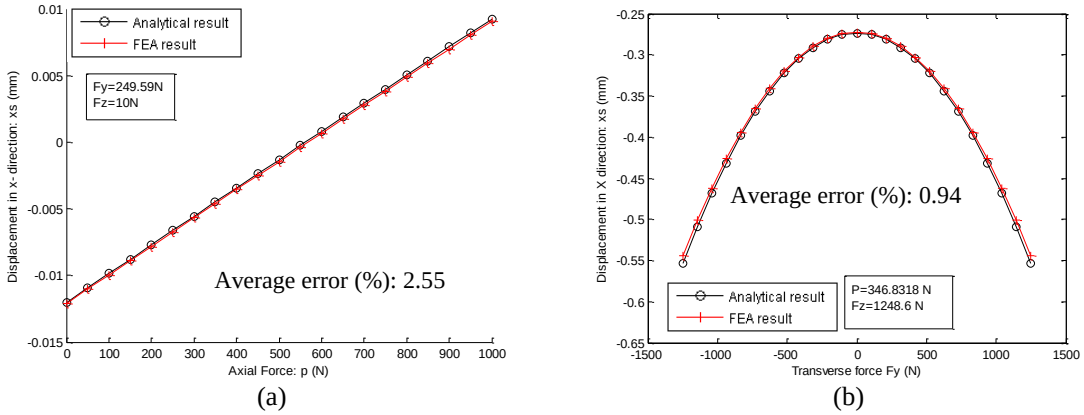

(a) (b)

Fig. 8 Axial displacement verification: (a) for different P, (b) for different F_y.

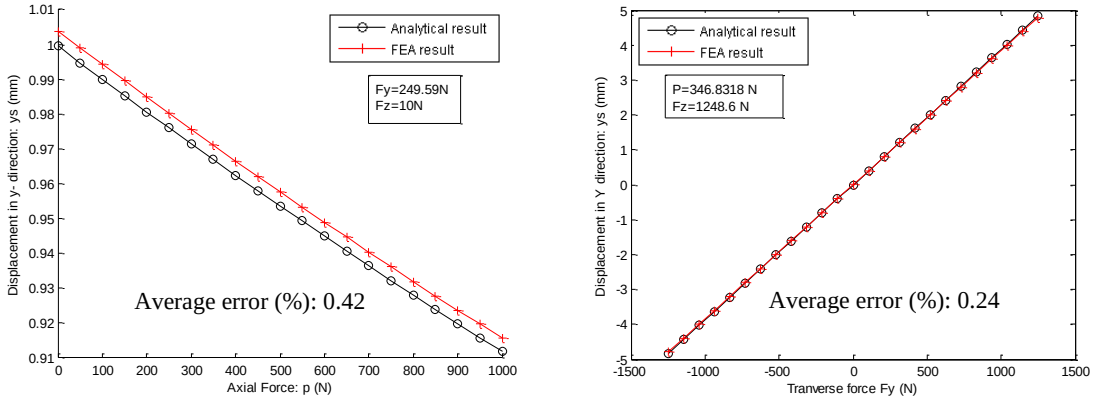

Fig. 9 Y displacement verification: (a) cross-axis coupling from different *P*, (b) primary stiffness.

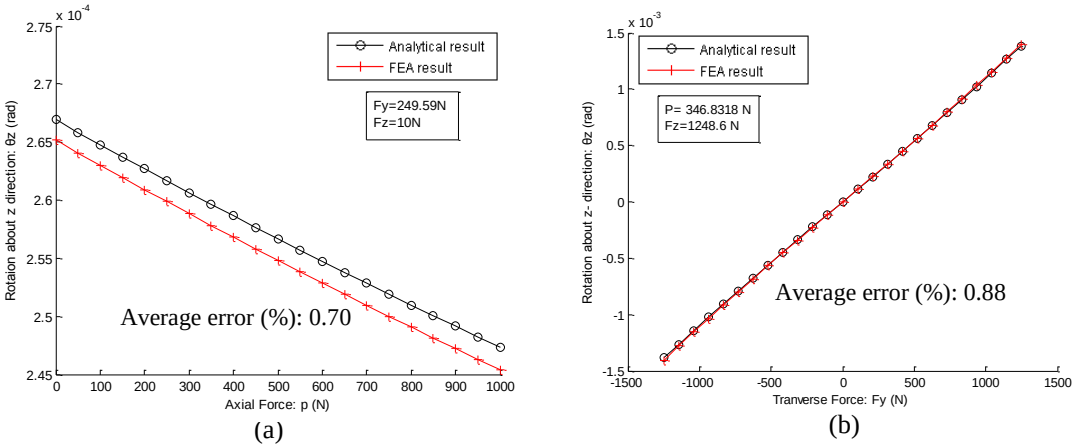

Fig. 10 Bending angle about the *Z*-axis: (a) for different *P*, (b) for different F_y.

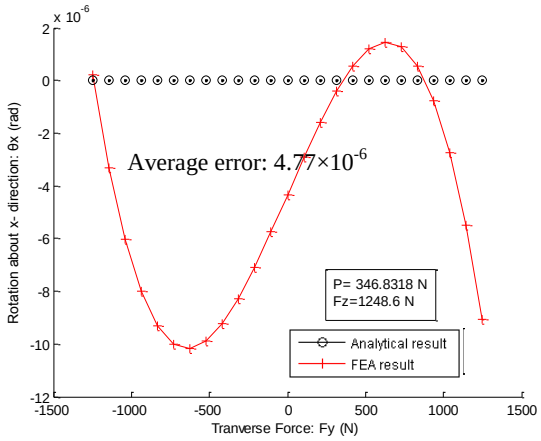

Fig. 11 Torsional angle for different F_y.

If only the torsional moment, $M_x=GI_p/L=1.3069\times10^4$ Nmm, is imposed on the motion stage, the analytical result using Eq. (36) and FEA result of the rotational angle θ_{sx} are respectively 0.0495 radians and 0.0494 radians, an error of about 0.2%.

A prototype of a three-beam module, made of engineering plastic, have been fabricated using 3-D printer for initial qualitative analysis (see Appendix C for details). The preliminary test results with the prototype comply with the modeling presented in this paper.

5. Multi-beam spatial module analysis

In this section, we will deal briefly with multi-beam modules with more than three beams only having three in-plane DOF, in particular five classes of multi-beam module with different layouts of beams. As in the case of the three-beam spatial module, the loads are taken to be acting at the center of motion stage, and the coordinate system, displacements and loads are defined in the same way. Figure 12 shows six-beam spatial modules with a variety of layouts.

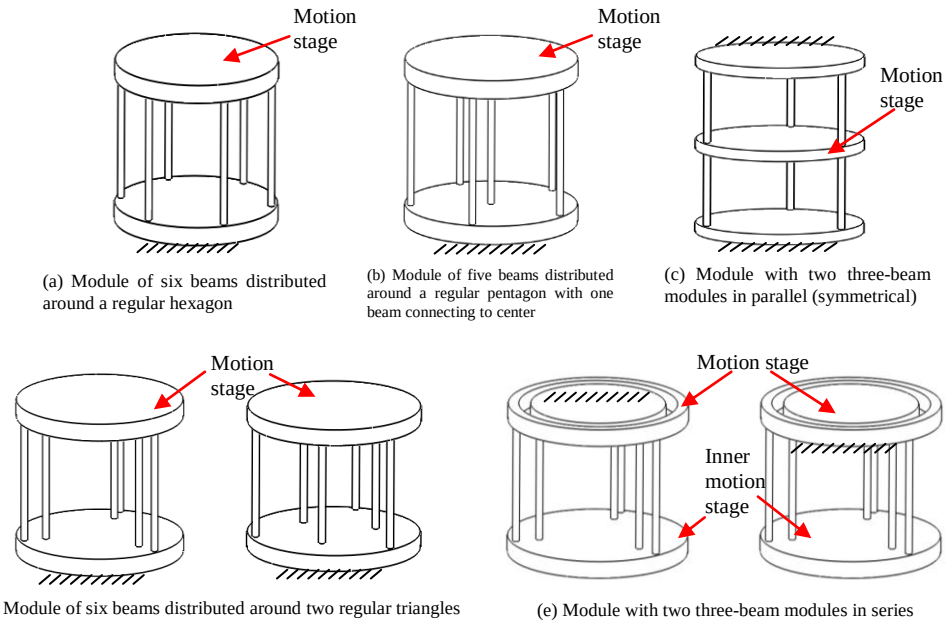

(a) Module of six beams distributed around a regular hexagon

(b) Module of five beams distributed around a regular pentagon with one beam connecting to center

(c) Module with two three-beam modules in parallel (symmetrical)

(d) Module of six beams distributed around two regular triangles

(e) Module with two three-beam modules in series

Fig. 12 Six-beam spatial modules with round cross-section beams.

In the following, we limit ourselves to multi-beam spatial modules, which have an even number of beams, *n*, and in which all beams are uniformly distributed around a circle [Fig. 12(a)]. Apparently, the multi-beam module has good dynamic performance of high band-width and large buckling load with the increasing of the number of beams, but in turn results in large primary motion stiffness.

The approximate analytical load-displacement equations for a motion stage in four-beam and six-beam spatial modules can be obtained in a similar way to the approximate analytical model for the three-beam module:

$$\begin{cases} \theta_{sx} \approx \dfrac{m_x\delta + (m_z f_z + m_y f_y)e/(4a+pe)}{4(\delta + ar_4^2 + \dfrac{p}{4}er_4^2)} \\ y_s \approx \dfrac{f_y + m_y\theta_{sx}e}{4a+pe} \\ z_s \approx \dfrac{f_z + m_z\theta_{sx}e}{4a+pe} \\ \theta_{sy} \approx \dfrac{1}{2r_4^2}(\dfrac{1}{d} + y_s^2 r + z_s^2 r)[m_y + (4c+ph)z_s] - 2\theta_{sx}y_s i \\ \theta_{sz} \approx \dfrac{1}{2r_4^2}(\dfrac{1}{d} + y_s^2 r + z_s^2 r)[m_z - (4c+ph)y_s] - 2\theta_{sx}z_s i \\ x_s \approx \dfrac{p}{4d} + (y_s^2 + z_s^2)i + \dfrac{p}{4}(y_s^2 + z_s^2)r + r_4^2\theta_{sx}^2 i + \dfrac{p}{4}r_4^2\theta_{sx}^2 r + 2(y_s\theta_{sz} - z_s\theta_{sy})k - \dfrac{1}{2}(m_y y_s + m_z z_s)\theta_{sx}r \end{cases} \tag{67}$$

$$\begin{cases} \theta_{sx} \approx \dfrac{m_x\delta + (m_z f_z + m_y f_y)e/(6a+pe)}{6(\delta + ar_6^2 + \dfrac{p}{6}er_6^2)} \\ y_s \approx \dfrac{f_y + m_y\theta_{sx}e}{6a+pe} \\ z_s \approx \dfrac{f_z + m_z\theta_{sx}e}{6a+pe} \\ \theta_{sy} \approx \dfrac{1}{3r_6^2}(\dfrac{1}{d} + y_s^2 r + z_s^2 r)[m_y + (6c+ph)z_s] - 2\theta_{sx}y_s i \\ \theta_{sz} \approx \dfrac{1}{3r_6^2}(\dfrac{1}{d} + y_s^2 r + z_s^2 r)[m_z - (6c+ph)y_s] - 2\theta_{sx}z_s i \\ x_s \approx \dfrac{p}{6d} + (y_s^2 + z_s^2)i + \dfrac{p}{6}(y_s^2 + z_s^2)r + r_6^2\theta_{sx}^2 i + \dfrac{p}{6}r_6^2\theta_{sx}^2 r + 2(y_s\theta_{sz} - z_s\theta_{sy})k - \dfrac{1}{3}(m_y y_s + m_z z_s)\theta_{sx}r \end{cases} \tag{68}$$

The general load-displacement equations for spatial multi-beam modules can be summarized as follows:

$$
\begin{cases}
\theta_{sx} \approx \dfrac{m_x\delta + (m_z f_z + m_y f_y)e/(na+pe)}{n(\delta + ar_n^2 + \dfrac{p}{n}er_n^2)} \\
y_s \approx \dfrac{f_y + m_y\theta_{sx}e}{na+pe} \\
z_s \approx \dfrac{f_z + m_z\theta_{sx}e}{na+pe} \\
\theta_{sy} \approx \dfrac{1}{4r_n^2 \sum\limits_{i_0=1(odd)}^{n/2} [\cos\dfrac{i_0\pi}{n}]^2}(\dfrac{1}{d} + y_s^2 r + z_s^2 r)[m_y + (nc+ph)z_s] - 2\theta_{sx}y_s i \\
\quad = \dfrac{2}{nr_n^2}(\dfrac{1}{d} + y_s^2 r + z_s^2 r)[m_y + (nc+ph)z_s] - 2\theta_{sx}y_s i \\
\theta_{sz} \approx \dfrac{1}{4r_n^2 \sum\limits_{i_0=1(odd)}^{n/2} [\sin\dfrac{i_0\pi}{n}]^2 - j_0 2r_n^2}(\dfrac{1}{d} + y_s^2 r + z_s^2 r)[m_z - (nc+ph)y_s] - 2\theta_{sx}z_s i \\
\quad = \dfrac{2}{nr_n^2}(\dfrac{1}{d} + y_s^2 r + z_s^2 r)[m_z - (nc+ph)y_s] - 2\theta_{sx}z_s i \\
x_s \approx \dfrac{p}{nd} + (y_s^2 + z_s^2)i + \dfrac{p}{n}(y_s^2 + z_s^2)r + r_n^2\theta_{sx}^2 i + \dfrac{p}{n}r_n^2\theta_{sx}^2 r + 2(y_s\theta_{sz} - z_s\theta_{sy})k - \dfrac{2}{n}(m_y y_s + m_z z_s)\theta_{sx} r
\end{cases}
\tag{69}
$$

where, $j_0 = \begin{cases} 0 & \text{for} \quad n/4 = \text{int} \\ 1 & \text{for} \quad n/4 \neq \text{int} \end{cases}$, the beam number n is even and $n < \dfrac{2\pi r_n}{D_0/L}$, r_n denotes the nondimensional pitch circle radius of the beam tips. If the torque is normalized by EI/L, the torsional angle becomes

$$\theta_{sx} \approx [m_x + (m_z f_z + m_y f_y)e/(na+pe)]/[n(\delta + ar_n^2 + \frac{p}{n}er_n^2)].$$

The system shown in Fig. 12(c) is obtained by symmetrically arranging two three-beam modules as two building blocks. This system is kinematicly decoupled in two transverse translational directions, and has a large load-stiffening effect, resulting from the augmentation of transverse stiffness in the presence of gradually increased axial tension-force in the configuration of two symmetrical three-beam modules, as shown in the transverse displacement equations [Eqs. (33) and (34)]. The system shown in Fig. 12(e) is obtained by connecting two three-beam modules as two building blocks in series. This system has approximately half the primary stiffness and double the motion range of the single three-beam module, and can alleviate the load-stiffening effect.

6. Conclusions

The nonlinear and analytical load-displacement equations of the spatial multi-beam CPMs, with round or regular polygon cross-section beams have been formulated and analyzed by mathematical transformation and substitution. A method has also been presented to analyze the spatial combined deformation of compliant beams or mechanisms.

For a set of given payloads exerted on the motion stage of the spatial three-beam module, one can obtain quickly the displacements using the proposed nonlinear models as compared with FEA or other numerical methods. The larger the pitch circle radius of beam tips, the smaller the absolute value of the torsional angle and therefore the more accurate the proposed approximate analytical model. It has been verified using the large-deflection FEA that the accuracy of the proposed analytical model is acceptable. In the case of our example CPM, the maximum transverse displacements for the proposed spatial modules are approximately 5.0 mm (0.1*L*) under small deflection's condition.

An analysis of the modules proposed in Figs. 12(b) – (e) and a comparison between experiment results at the macro- and micro-scale and analytical results will be areas for further investigation.

References

[1] J.P. Merlet, Parallel Robotics, Springer, Berlin, 2006.
[2] X. Kong, and C.M. Gosselin, Type Synthesis of Parallel Mechanisms, Springer, Berlin, 2007.
[3] N. Lobontiu, Compliant Mechanisms: Design of Flexure Hinges, CRC PRESS, 2002.
[4] L.L. Howell, Compliant Mechanisms, Wiley, New York, 2001.
[5] S. Awtar, Analysis and Synthesis of Planer Kinematic XY Mechanisms, Sc.D. thesis, Massachusetts Institute of Technology, Cambridge, MA, 2004.
[6] S. Kota, K.-J. Lu, Z. Kreiner, and et al, Design and Application of Compliant Mechanisms for Surgical Tools, Journal of Biomechanical Engineering 127 (6) (2005) 981-989
[7] G. Krishnan, and G.K. Ananthasuresh, Evaluation and Design of Displacement-Amplifying Compliant Mechanisms for Sensor Applications, Journal of Mechanical Design 130 (10) (2008) 102304.1-102304.9.

[8] J. Li, Electrostatic Zipping Actuators and Their Application to MEMS, Sc.D. thesis, Massachusetts Institute of Technology, Cambridge, MA, 2004.
[9] Q.S. Xu, and Y.M. Li, Design of a Partially Decoupled High Precision XYZ Compliant Parallel Micromanipulator, Proceedings of the 3rd IEEE International Conference on Nano/Micro Engineered and Molecular Systems, Sanya, China, January 6-9, 2008, pp. 13-18.
[10] Y. Wang, and C.M. Gosselin, On the Design of a 3-PRRR Spatial Parallel Compliant Mechanism, Proceeding of the ASME 28th Biennial Mechanisms and Robotics Conference, Salt Lake City, Utah, USA, Sep. 28 –Oct. 2, 2004. DETC2004-57140
[11] H.-H. Pham, H.C. Yeh, and I.-M. Chen, Micromanipulation System Design Based on Selective Actuation Mechanisms, The International Journal of Robotics Research, 25 (2) (2006) 171-186.
[12] H. Zhou, and K.L. Ting, Geometric Modeling and Synthesis of Spatial Multimaterial Compliant Mechanisms and Structures Using Three-Dimensional Multilayer Wide Curves, Journal of Mechanical Design, 131 (1) (2009) 011005.1-011005.8.
[13] H. Zhou, and K.L. Ting, Geometric Modeling and Optimization of Multimaterial Compliant Mechanisms Using Multilayer Wide Curves, Journal of Mechanical Design, 130 (6) (2009) 062303.1-062303.7.
[14] K.-J. Lu, and S. Kota, Topology and Dimensional Synthesis of Compliant Mechanisms Using Discrete Optimization, Journal of Mechanical Design, 128 (9) (2006) 1080-1090.
[15] S. Awtar, and A.H. Slocum, Constraint-Based Design of Parallel Kinematic XY Flexure Mechanisms, Journal of Mechanical Design, 129 (8) (2007) 816-830.
[16] K.-B. Choi, and J.J. Lee, Analysis and Design Linear Parallel Stage for Ultra-Precision Motion Based on 4-PP Flexural Joint Mechanism, International Conference on Smart Manufacturing Application, KINTEX, Gyeonggi-do, Korea, April. 9-11, 2008, pp. 35-38.
[17] C.J. Kim, Y.M. Moon, and S. Kota, A Building Block Approach to the Conceptual Synthesis of Compliant Mechanisms Utilizing Compliance and Stiffness Ellipsoids, Journal of Mechanical Design, 130 (2) (2008) 022308.1-022308.11.
[18] H.-J. Su, D.V. Dorozhkin, and J.M. Vance, A Screw Theory Approach for the Conceptual Design of Flexible Joints for Compliant Mechanisms, Journal of Mechanisms and Robotics, 1 (4) (2009) 041009.
[19] J.B. Hopkins, and M.L. Culpepper, Synthesis of Multi-Degree of Freedom, Parallel Flexure System Concepts via Freedom and Constraint Topology (FACT). Part I: Principles, Precision Engineering, 34 (1) (2010) 259-270.
[20] J.B. Hopkins, and M.L. Culpepper, Synthesis of Multi-Degree of Freedom, Parallel Flexure System Concepts via Freedom and Constraint Topology (FACT). Part II: Practice, Precision Engineering, 34 (1) (2010) 271-278.
[21] S.P. Timoshenko, and J.M. Gere, Theory of elastic stability, 2nd ed. New York: McGraw-Hill, 1961.
[22] S. Zelenika, and F. De Bona, Analytical and Experimental Characterization of High-Precision Flexural Pivots Subjected to Lateral Loads, Precision Engineering, 26 (4) (2002) 381-388.
[23] S. Awtar, and A.H. Slocum, Characteristics of Beam-Based Flexure Modules", Journal of Mechanical Design, 129 (6) (2007) 624-639.
[24] E.J. Hearn, Mechanics of Materials, Robert Maxwell, M. C. Pergamon Press, Oxford, 1983.
[25] L. Nicolae, S.L.P. Jeffrey, G. Ephrahim, and G. Michael, Corner-Filleted Flexure Hinges, Journal of Mechanical Design, 123 (2001) 346-352.
[26] J. Ryu, S.-S. Kim, and S.-S. Kim, A Criterion on Inclusion of Stress Stiffening Effects in Flexible Multibody Dynamic System Simulation, Computers & Structures, 62 (6) (1997) 1035-1048.
[27] S. Awtar, and E. Sevincer, Elastic Averaging in Flexure Mechanisms: A Three-Beam Parallelogram Flexure Case Study", Journal of Mechanisms and Robotics, 2 (4) (2010) 041005.
[28] G. Hao, and X. Kong, A 3-DOF Translational Compliant Parallel Manipulator Based on Flexure Motion, Proceedings of 2009 ASME International Design Engineering Technical Conferences& Computers and Information in Engineering Conference, San Diego, CA, USA, Aug. 30-Sep. 2, 2009, pp.1-11. DETC2009-86075
[29] J.S. Dai, and X.L. Ding, Compliance Analysis of a Three-Legged Rigidly-Connected Platform Device, Journal of Mechanical Design, 128 (6) (2006) 755-764.
[30] X.L. Ding, and J.S. Dai, Characteristic Equation-Based Dynamics Analysis of Vibratory Bowl Feeders with Three Spatial Compliant Legs, IEEE Transactions on Robotics and Automation, 5 (1) (2006) 164-175.
[31] H. D. Samuel, and N. S.Sergio, Compliant Assembly System, United States patent, No.: 4155169, 1979.
[32] G. Hao, X. Kong, and Q. Meng, Design and Modelling of Spatial Compliant Parallel Mechanisms for Large Range of Translation, Proceedings of 2010 ASME International Design Engineering Technical Conferences& Computers and Information in Engineering Conference, Montréal, Québec, Canada, Aug. 15-18, 2010. DETC2010-28046.
[33] G. Hao, and X. Kong, Novel XY Compliant Parallel Manipulators for Large Displacement Translation with Enhanced Stiffness, Proceedings of 2010 ASME International Design Engineering Technical Conferences& Computers and Information in Engineering Conference, Montréal, Québec, Canada, Aug. 15-18, 2010. DETC2010-28141
[34] B.P. Trease, Y.-M. Moon, and S. Kota, Design of Large-Displacement Compliant Joints, Journal of Mechanical Design, 127 (7) (2005) 788-798.
[35] X. Pei, J. Yu, G. Zong, and et al, A Novel Family of Leaf-Type Compliant Joints: Combination of Two isosceles-Trapezoidal Flexural Pivots, Journal of Mechanism and Robotics, 1 (2) (2009) 1-6.
[36] J.B. Hopkins, and M.L. Culpepper, A Screw Theory Basis for Quantitative and Graphical Design Tools That Define Layout of Actuators to Minimize Parasitic Errors in Parallel Flexure Systems, Precision Engineering, 34 (4) (2010) 767-776.
[37] J.B. Kuipers, Quaternions and Rotation Sequences, Princeton University Press, US, 2002.
[38] S.P. Salisbury, and R. Ben Mrad, Analytical Stiffness Estimation for Short Flexures, Mechatronics, 16 (7) (2006) 399–403.

Appendices

A. Nonlinear analysis of a beam for the bending only in the XY (XZ) plane

Figure A1 shows a deformed beam for the bending only in XY plane.

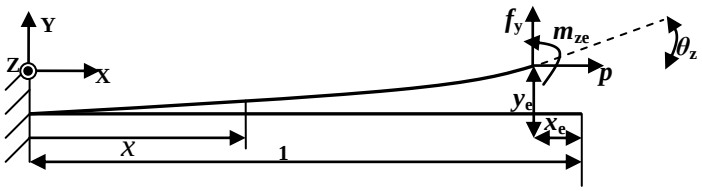

Fig. A1 Deformation of a beam.

Based on the Euler's formula and load equilibrium condition after deformation, we can obtain the differential equation of a beam under small deflection as

$$y''(x) = m_{ze} + f_y(1 + x_e - x) - p[y_e - y(x)]$$

where $m_{ze} + f_y(1 + x_e - x) - p[y_e - y(x)]$ is the bending moment acting at any x location of the beam about the Z-axis; m_{ze}, f_y and p are, respectively, the bending moment about the Z-axis, the transverse force along the Y-axis and the axial force along the X-axis acting at the free-end of the beam; y_e and x_e are, respectively, the transverse displacement along the Y-axis and axial displacement along the X-axis of the free-end of the beam; $y(x)$ is the transverse displacement of any x location on the beam along the Y-axis. The subscript e denotes the free-end.

The above equation can be rewritten as

$$y''(x) - py(x) = m_{ze} + f_y(1 + x_e - x) - py_e \tag{A. 1}$$

The boundary conditions for Eq. (A. 1) are

y=0 when x=0;

y'=0 when x=0. (A. 2)

Awtar [5] used a homogeneous 4th-order differential equation, obtained by differentiating Eq. (A. 1) with respect to x twice, to solve load-displacement equations.

This appendix presents alternative solution to Eq. (A1) (non-homogeneous 2nd-order differential equation) directly by combining the general solution to the corresponding homogeneous differential equation and the particular solution to the non-homogeneous differential equation.

The general solution to the corresponding homogeneous differential equation ($y'' - py = 0$) is

$$y = Ae^{kx} + B^{-kx} \tag{A. 3}$$

where k^2=p.

The particular solution to the non-homogeneous differential equation is assumed as

$$y=Cx+D \tag{A. 4}$$

Substituting Eq. (A. 4) into the Eq. (A. 1), we can obtain

$$-k^2(Cx + D) = m_{ze} + f_y(1 + x_e) - k^2 y_e - f_y x$$

Then we have

$$\begin{cases} -k^2 C = -f_y \\ -k^2 D = m_{ze} + f(1 + x_e) - k^2 y_e \end{cases}$$

i.e.

$$\begin{cases} C = f_y / k^2 \\ D = -\dfrac{m_{ze} + f_y(1 + x_e) - k^2 y_e}{k^2} \end{cases} \tag{A. 5}$$

Combining Eqs. (A. 3), (A. 4) and (A. 5), we can obtain the general solution to the non-homogeneous 2-order differential equation as

$$y = Ae^{kx} + B^{-kx} + \frac{f_y}{k^2}x - \frac{m_{ze} + f_y(1 + x_e) - k^2 y_e}{k^2} \tag{A. 6}$$

Substituting the boundary condition, Eq. (A. 2), into Eq. (A. 6), we can obtain

$$A + B - \frac{m_{ze} + f_y(1 + x_e) - k^2 y_e}{k^2} = 0$$

$$Ak - Bk + \frac{f_y}{k^2} = 0$$

Solving the above equations, we then obtain

$$\begin{cases} A=\dfrac{1}{2}\left(\dfrac{m_{ze}+f_y(1+x_e)-k^2y_e}{k^2}-\dfrac{f_y}{k^3}\right) \\ B=\dfrac{1}{2}\left(\dfrac{m_{ze}+f_y(1+x_e)-k^2y_e}{k^2}+\dfrac{f_y}{k^3}\right) \end{cases} \tag{A. 7}$$

Substituting Eqs. (A. 5) and (A. 7) into Eq. (A. 6), the general solution to Eq. (A. 1) is obtained as

$$\begin{aligned} y(x) &= \frac{m_{ze}+f_y(1+x_e)-k^2y_e}{k^2}\left(\frac{e^{kx}+e^{-kx}}{2}\right)-\frac{f_y}{k^3}\left(\frac{e^{kx}-e^{-kx}}{2}\right)+\frac{f_y}{k^2}x-\frac{m_{ze}+f_y(1+x_e)-k^2y_e}{k^2} \\ &= \frac{m_{ze}+f_y(1+x_e)-k^2y_e}{k^2}\cosh kx-\frac{f_y}{k^3}\sinh kx+\frac{f_y}{k^2}x-\frac{m_{ze}+f_y(1+x_e)-k^2y_e}{k^2} \end{aligned} \tag{A. 8}$$

An analogous solution can also be obtained in terms of trigonometric functions rather than the above hyperbolic functions for negative values of p.

When x=1, the transverse displacement y_e and the rotational angle θ_z about the Z-axis of the free-end can be obtained using Eq. (A. 8) as

$$y_e = y(1) \approx \frac{m_{ze}+f_y-k^2y_e}{k^2}\cosh k-\frac{f_y}{k^3}\sinh k+\frac{f_y}{k^2}-\frac{m_{ze}+f_y-k^2y_e}{k^2}$$

i.e.

$$y_e = \frac{f_y(k-\tanh k)}{k^3}+\frac{m_{ze}(\cosh k-1)}{k^2\cosh k} \tag{A. 9}$$

$$\theta_z = y'(1) \approx \frac{m_{ze}+f_y-k^2y_e}{k}\sinh k-\frac{f_y}{k^2}\cosh k$$

i.e.

$$\theta_z = \frac{f_y(\cosh k-1)}{k^2\cosh k}+\frac{m_{ze}\tanh k}{k} \tag{A. 10}$$

Equations (A. 9) and (A. 10) are same as the results derived in [5, 23].

As in [5], the axial displacement can be divided in two parts: a purely elastic component and a kinematic component as

$$x_e = \delta_x^e + \delta_x^k$$

where $\delta_x^e = p/d$, which is the purely elastic component, δ_x^k is the kinematic component.

The kinematic component can be obtained as follows:

$$\mathrm{d}s = \mathrm{d}x/\cos\theta = (1+\tan^2\theta)^{1/2}\,\mathrm{d}x = (1+y'^2)^{1/2}\,\mathrm{d}x \approx (1+\frac{1}{2}y'^2)\,\mathrm{d}x$$

Then we obtain

$$\int_0^{1+\delta_x^e}\mathrm{d}s = \int_0^{1+x_e}(1+\frac{1}{2}y'^2)\,\mathrm{d}x$$

i.e.

$$1+\delta_x^e = 1+(\delta_x^e+\delta_x^k)+\frac{1}{2}\int_0^1 y'^2\,\mathrm{d}x$$

Then above equation can be rewritten as

$$\delta_x^k = -\frac{1}{2}\int_0^1 y'^2\,\mathrm{d}x \tag{A. 11}$$

Substituting Eq. (A. 8) into Eq. (A. 11) and combining with the purely elastic component, we can obtain the axial displacement (see [5] for detailed expression).

Then making approximations for all load-displacement equations of the free-end of the beam based on the Taylor series expansion, we obtain

$$\begin{bmatrix} f_y \\ m_{ze} \end{bmatrix} = \begin{bmatrix} a & c \\ c & b \end{bmatrix}\begin{bmatrix} y_e \\ \theta_z \end{bmatrix} + p\begin{bmatrix} e & h \\ h & g \end{bmatrix}\begin{bmatrix} y_e \\ \theta_z \end{bmatrix} + p^2\begin{bmatrix} -1/700 & 1/1400 \\ 1/1400 & -11/6300 \end{bmatrix}\begin{bmatrix} y_e \\ \theta_z \end{bmatrix}+\cdots \tag{A. 12a}$$

$$x_e = \frac{1}{d}p + [y_e,\theta_z]\begin{bmatrix} i & k \\ k & j \end{bmatrix}\begin{bmatrix} y_e \\ \theta_z \end{bmatrix} + p[y_e,\theta_z]\begin{bmatrix} r & q \\ q & s \end{bmatrix}\begin{bmatrix} y_e \\ \theta_z \end{bmatrix} + p^2[y_e,\theta_z]\begin{bmatrix} 1/42000 & -1/84000 \\ -1/84000 & 1/18000 \end{bmatrix}\begin{bmatrix} y_e \\ \theta_z \end{bmatrix}+\cdots \tag{A. 12b}$$

Similarly, the load-displacement equations of the free-end of a beam for the bending only in the XZ plane can be obtained as

$$\begin{bmatrix} f_z \\ -m_{ye} \end{bmatrix} = \begin{bmatrix} a & c \\ c & b \end{bmatrix}\begin{bmatrix} z_e \\ -\theta_y \end{bmatrix} + p\begin{bmatrix} e & h \\ h & g \end{bmatrix}\begin{bmatrix} z_e \\ -\theta_y \end{bmatrix} + p^2\begin{bmatrix} -1/700 & 1/1400 \\ 1/1400 & -11/6300 \end{bmatrix}\begin{bmatrix} z_e \\ -\theta_y \end{bmatrix}+\cdots \tag{A. 13a}$$

$$x_e = \frac{1}{d}p + [z_e,-\theta_y]\begin{bmatrix} i & k \\ k & j \end{bmatrix}\begin{bmatrix} y_e \\ -\theta_y \end{bmatrix} + p[z_e,-\theta_y]\begin{bmatrix} r & q \\ q & s \end{bmatrix}\begin{bmatrix} z_e \\ -\theta_y \end{bmatrix} + p^2[z_e,-\theta_y]\begin{bmatrix} 1/42000 & -1/84000 \\ -1/84000 & 1/18000 \end{bmatrix}\begin{bmatrix} z_e \\ -\theta_y \end{bmatrix}+\cdots \tag{A. 13b}$$

where m_{ye}, f_z and p are, respectively, the bending moment about the Y-axis, the transverse force along the Z-axis and the axial force along the X-axis acting at the free-end of the beam; z_e, x_e and θ_y are, respectively, the transverse displacement along the Z-axis, the axial displacement along the X-axis and the rotational angle about the Y-axis of the free-end of the beam.

B. Torsion of a beam after deformation about the X-axis

Due to the small deflection hypothesis, we can assume

$$\mathrm{d}\theta_x = m_x(x)\mathrm{d}x \tag{B. 1a}$$

where $m_x(x) = m_{xe} + f_z[y_e - y(x)]/\delta - f_y[z_e - z(x)]/\delta$, which is the torque acting at any x location on the beam about the X-axis in deformed configuration; δ=2G/E; m_{xe}, f_z, and f_y are, respectively, the torque about the X-axis, the transverse force along the Z-axis and the transverse force along the Y-axis acting at the free-end of the beam; y_e and z_e are the transverse displacements of the free-end of the beam along the Y- and Z-axes, respectively; $y(x)$ and $z(x)$ are the transverse displacements of any x location on the beam along the Y- and Z-axes, respectively.

Equation (B. 1a) can be rewritten as

$$\mathrm{d}\theta_x = \{m_{xe} + f_z[y_e - y(x)]/\delta - f_y[z_e - z(x)]/\delta\}\mathrm{d}x \tag{B. 1b}$$

Based on Eq. (A. 8), $y(x)$ and $z(x)$ can be expressed respectively as

$$\begin{aligned} y(x) &= \frac{m_{ze} + f_y - k^2 y_e}{k^2}\cosh kx - \frac{f_y}{k^3}\sinh kx + \frac{f_y}{k^2}x - \frac{m_{ze} + f_y - k^2 y_e}{k^2} \\ z(x) &= \frac{-m_{ye} + f_z - k^2 z_e}{k^2}\cosh kx - \frac{f_z}{k^3}\sinh kx + \frac{f_z}{k^2}x - \frac{-m_{ye} + f_z - k^2 z_e}{k^2} \end{aligned} \tag{B. 2}$$

where k^2=p. p, m_{ye} and m_{ze} are, respectively, the axial force along the X-axis, the bending moment about the Y-axis and the bending moment about the Z-axis acting at the free-end of the beam.

The torsional angle of free-end can be obtained by integrating Eq. (B. 1b) as

$$\theta_x = \int_0^1 \{m_{xe} + f_z[y_e - y(x)]/\delta - f_y[z_e - z(x)]/\delta\}\mathrm{d}x = m_{xe} + (f_z y_e - f_y z_e)/\delta - \int_0^1 [f_z y(x)/\delta - f_y z(x)/\delta]\mathrm{d}x$$

Substituting Eq. (B. 2) into the above equation, we obtain

$$\begin{aligned} \theta_x = m_{xe} &+ (f_z y_e - f_y z_e)/\delta - \int_0^1 \{f_z[\frac{m_{ze} + f_y - k^2 y_e}{k^2}\cosh kx - \frac{f_y}{k^3}\sinh kx + \frac{f_y}{k^2}x - \frac{m_{ze} + f_y - k^2 y_e}{k^2}]/\delta \\ &- f_y[\frac{-m_{ye} + f_z - k^2 z_e}{k^2}\cosh kx - \frac{f_z}{k^3}\sinh kx + \frac{f_z}{k^2}x - \frac{-m_{ye} + f_z - k^2 z_e}{k^2}]/\delta\}\mathrm{d}x \end{aligned} \tag{B. 3}$$

We take the third term in Eq. (B. 3) for further simplification as follows:

$$\begin{aligned} &\int_0^1 \{f_z[\frac{m_{ze} + f_y - k^2 y_e}{k^2}\cosh kx - \frac{f_y}{k^3}\sinh kx + \frac{f_y}{k^2}x - \frac{m_{ze} + f_y - k^2 y_e}{k^2}]/\delta \\ &- f_y[\frac{-m_{ye} + f_z - k^2 z_e}{k^2}\cosh kx - \frac{f_z}{k^3}\sinh kx + \frac{f_z}{k^2}x - \frac{-m_{ye} + f_z - k^2 z_e}{k^2}]/\delta\}\mathrm{d}x \\ &= (f_z y_e - f_y z_e)/\delta + \int_0^1 \{[\frac{f_z m_{ze} - f_z k^2 y_e}{k^2}\cosh kx - \frac{f_z m_{ze}}{k^2}]/\delta - [\frac{-f_y m_{ye} - f_y k^2 z_e}{k^2}\cosh kx - \frac{-f_y m_{ye}}{k^2}]/\delta\}\mathrm{d}x \\ &= (f_z y_e - f_y z_e)/\delta + \int_0^1 \{[\frac{f_z m_{ze} - f_z k^2 y_e}{k^2} - \frac{-f_y m_{ye} - f_y k^2 z_e}{k^2}]\cosh kx/\delta + [\frac{-f_y m_{ye}}{k^2} - \frac{f_z m_{ze}}{k^2}]/\delta\}\mathrm{d}x \\ &= (f_z y_e - f_y z_e)/\delta + [(\frac{f_z m_{ze} + f_y m_{ye}}{k^2} + f_y z_e - f_z y_e)/\delta]\sinh k/k + (\frac{-f_y m_{ye} - f_z m_{ze}}{k^2})/\delta \end{aligned} \tag{B. 4}$$

According to the Taylor series expansion, we have

$$e^k = 1 + k + k^2/2 + \cdots + k^n/n! + \cdots$$

Thus

$$\sinh k/k = \frac{e^k - e^{-k}}{2k} = \frac{(1 + k + k^2/2 + \cdots) - (1 - k + k^2/2 + \cdots)}{2k} \approx 1 \tag{B. 5}$$

Substituting Eq. (B. 5) into (B. 4), and substituting the result into Eq. (B.3), we obtain

$$\begin{aligned} \theta_x &= m_{xe} + (f_z y_e - f_y z_e)/\delta - \{(f_z y_e - f_y z_e)/\delta + [(\frac{f_z m_{ze} + f_y m_{ye}}{k^2} + f_y z_e - f_z y_e)/\delta] + (\frac{-f_y m_{ye} - f_z m_{ze}}{k^2})/\delta\} \\ &= m_{xe} + (f_z y_e - f_y z_e)/\delta + 0 \end{aligned} \tag{B. 6}$$

Equation (B. 6) can also be explained qualitatively as follows. When we calculate the torsional angle θ_x, the beam can be assumed as a straight beam without bending deformations (Fig. B1). Therefore, the torsional moment $m_x(x)$, with respect to central axis of the undeformed beam, at any x location on the beam may be regarded as $m_{xe} + (f_z y_e - f_y z_e)/\delta$, and therefore the torsional angle can be also obtained as

$$\theta_x = \int_0^1 [m_{xe} + (f_z y_e - f_y z_e)/\delta]\mathrm{d}x = m_{xe} + (f_z y_e - f_y z_e)/\delta$$

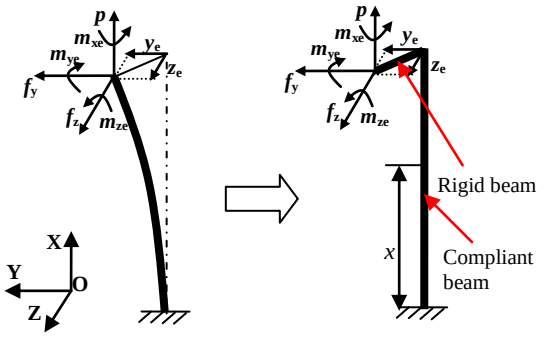

(a) Real configuration in deformation (b) Equivalent configuration

Fig. B1 Equivalent transformation for the torsional angle calculation.

Based on the mentioned principle of superposition in section 2.1, we can substitute Eqs. (A. 12a) and (A. 13a) into Eq. (B. 6) to obtain

$$\theta_x = m_{xe} + (f_z y_e - f_y z_e)/\delta = m_{xe} + (az_e + pez_e)y_e/\delta - (ay_e + pey_e)z_e/\delta - c(\theta_z z_e + \theta_y y_e)/\delta - ph(\theta_z z_e + \theta_y y_e)/\delta$$
$$= m_{xe} - c(\theta_z z_e + \theta_y y_e)/\delta - ph(\theta_z z_e + \theta_y y_e)/\delta \quad \text{(B. 7)}$$

C. Prototype of a three-beam module

A fabricated three-beam module under the action of f_z and m_x is shown in Fig. C1. Under the above payloads, the three-beam module has two primary motions: z_s and θ_{sx} [Fig. C1(a)]. In addition, the parasitic rotational angle of the motion stage about the Z-axis is dominated by $1.2z_s\theta_{sx}$ [see Eq. (29)], which can be verified by the experiment as shown in Fig. C1(b).

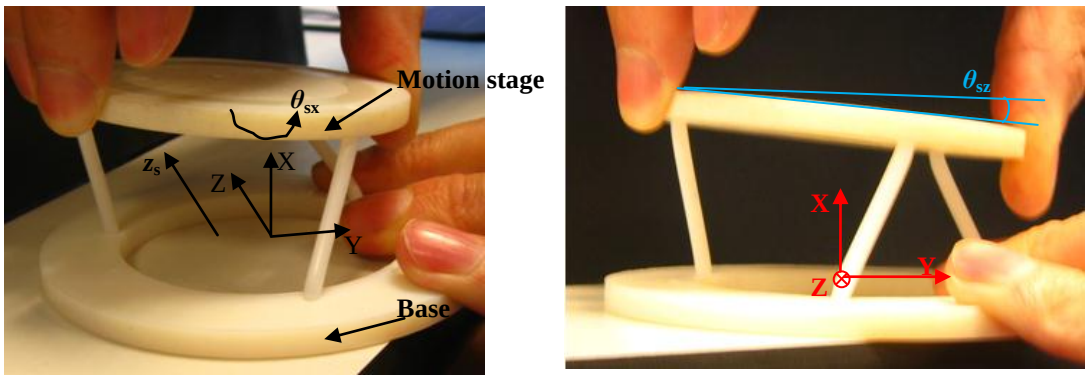

(a) (b)

Fig. C1 Prototype of a three-beam module in deformation.